Summer 2012

Sapphire fiber numerical aperture measurement and sensor fabrication

Xia Fang

Department:

SAPPHIRE FIBER NUMERICAL APERTURE MEASUREMENT AND SENSOR FABRICATION

by

XIA FANG

A THESIS

Presented to the Faculty of the Graduate School of the

MISSOURI UNIVERSITY OF SCIENCE AND TECHNOLOGY

In Partial Fulfillment of the Requirements for the Degree

MASTER OF SCIENCE IN ELECTRICAL ENGINEERING

2012

Approved by

Hai Xiao, Advisor
Hai-Lung Tsai
Kurt Kosbar

ABSTRACT

A sapphire fiber is made of single crystal aluminum oxide with hexagonal crystal structure. It is attractive for high temperature application for its chemical resistance and high melting point of 2053°C. It is good for infrared transmission with a small attenuation of 0.13dB per meter at the wavelength of 2.94μm, and it can also deliver very high optical energy. However, a typical sapphire fiber has a rough surface and a non-perfect crystalline structure. Also, a sapphire fiber cannot be grown in a core-clad structure. The un-cladded waveguide imposes a number of undesirable characteristics on sensing applications, e.g., unpredictable light loss and highly multimode operation. Therefore, a suitable cladding layer for sapphire fiber is highly desired for optimizing sapphire fiber optical properties.

This thesis aims to investigate the optical properties of single crystal sapphire fibers for development of high performance sensors for various high-temperature sensing applications. The numerical aperture of cladded and uncladded sapphire fibers were measured experimentally and compared for the purpose of selection of proper cladding materials. A novel assembly-free sapphire sensor probe was proposed for temperature and dynamic pressure measurement. The fabricated sensor probe successfully survived high temperatures upto 1560°C.

ACKNOWLEDGMENTS

I would like to take this opportunity to give my hearty gratitude to my supervisor, Dr. Hai Xiao, for whose encouragement, valuable guidance and support to me in this interesting and challenging research field. Without his determination and confidence, I would never have this great chance to carry out the most costly experiments in our lab. I would also like to thank Prof. Junhang Dong, who is from Department of Chemical Engineering of University of Cincinnati, for his help on my research work.

My gratitude should also be given to Dr. Hai-Lung Tsai, Department of Mechanical Engineering and Dr. Kurt Kosbar, Department of Electrical and Computer Engineering for serving on my committee.

I want to express my appreciation to my friends also cooperators, Hongmin Jiang, Department of Chemical Engineering, University of Cincinnati, and Yukun Han of Mechanical Engineering Department, for their unreserved help on my research work.
I would also like to thank all my colleagues and friends in Phonic Technology Lab. They are Dr. Qun Han, Dr. Wei Tao, Xinwei Lan, Amardeep Kuar, Yin Huang, Lei Yuan, Yinan Zhang, Pienkowski, Edward H., who has given me a lot good advices and kindly help.

I offer my regards and blessings to all of those who supported me in any respect during the way I pursing my Master degree. Without your help, this thesis would not have been possible finished.

Finally I would like to thank my husband, Baokai Cheng, who always stays with me wherever I will be and whatever problems I will meet, my parents who give me a life and raise me up, and my two sisters who make my life not lonely.

TABLE OF CONTENTS

LIST OF ILLUSTRATIONS

Page

LIST OF TABLES

Page

1. INTRODUCTION

While there has been a wealth of investigations in the field of low temperature fiber optic sensor fabricated in conventional silica glass fibers, the research area of high temperature fiber optic sensors is still immature. The chemical resistance and high melting point of sapphire fiber make it to be a potential candidate to replace the glass fibers in high temperature application.

The goal of this work is to investigate a proper cladding material for sapphire fiber and develop an assembly free sapphire fiber extrinsic Fabry-Perot (FP) sensor probe for measurement of high temperature. The highest expected operation temperature is around 1600 ^{o}C while, the softening point of single crystal sapphire fiber is 2053 ^{o}C .

Chapter 1 provides a briefly history introduction of optical fibers and presents the factors that limit the utilization of glass-based optical fiber sensors in high temperature. The sapphire fiber is then presented as an alternative to glass fiber for high-temperature sensing application.

1.1. HISTORY OF OPTICAL FIBERS

The principle that makes fiber optics possible, was first demonstrated by Daniel Colladon and Jacques Babinet in Paris in the early 1840s [1]. In 1910 Handros and Debye conducted a theoretical study and experimental work to investigate the electromagnetic waves propagating in dielectric wires [2]. However, the non-cladded waveguide proved to be an impractical waveguide due to its unsupported structure, especially when very thin waveguides were considered in order to limit the number of optical modes propagated. There were also excessive losses at any discontinuities of the glass-air interface. In 1950s, in order to solve this problem, scientist invented a cladding layer around the glass core. This structure efficiently reduces the radiation loss into the surrounding air, when the cladding is sufficiently thick. Around 1960s, the typical loss of fiber was over 1000dB/km, but Kao and Hockham[3] still believed that it was possible to reduce the loss and utilize optical fibers as a communications medium to transmit signals over a long distance and replace copper wires used for telecommunication. This idea was widely believed and led to a worldwide study to reduce the attenuation by purification of

the fiber materials. This effort has resulted in improved glass refining techniques to produce optical fibers with loss of around 4.2dB/km [4]. As the technique is improving, currently, the loss of typical silica fiber has been reduced to about 0.2dB/km.

1.2. SILICA OPTICAL FIBERS

Most existing optical fibers are manufactured for communication applications. Therefore, the low cost and low signal attenuation over distance becomes the major concerning parameters in manufacturing process. A common communication optical fiber is a flexible, transparent fiber made of very pure fused silica glass. The diameter of most glass fibers is 125um, which is comparable with human hair. A typical optical structure is shown in Figure 1.1. Glass fiber consists of a transparent core surrounded by a transparent cladding material with a lower index of refraction. The buffer outside the cladding layer is to protect fiber from physical damage and increase the flexibility of the glass fiber.

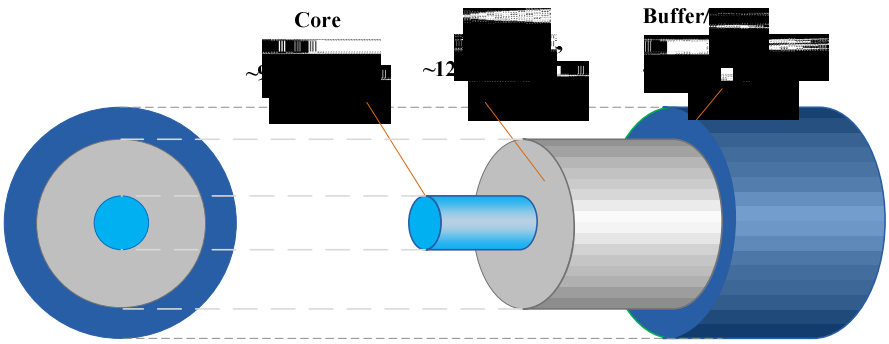

Figure 1.1. Typical structure of telecommunication optical fiber design

Through proper design of the waveguide structure, light signal can be kept in core of the optical fiber by total internal reflection. The ray propagation inside the fiber

waveguide is shown in Figure 1.2. , where n_c refers to the effective refractive index of cladding, n_f is the core effective refractive index and D is the core diameter.

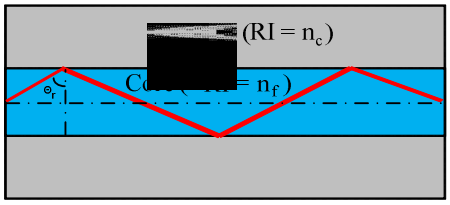

Figure 1.2. Propagation of a light ray in a fiber optical fiber

If the internal reflection angle of propagation ray θ_r is larger than the critical angle θ_c , which is defined by Equation.1.1, the light ray will be reflected back into the core at the core-cladding interface. Since the angles of incidence and reflection are always equal, the reflected light will again be reflected and travel forwards along the fiber core. However, if angle of internal reflection θ_r is less than the critical angle, then part of ray will be refracted into the cladding layer at core- cladding interface.

$$\theta_c = \sin^{-1}(\frac{n_c}{n_f}) \qquad (1.1)$$

1.3. SAPPHIRE OPTICAL FIBERS

A sapphire fiber is made of single crystal sapphire material with refractive index of approximately 1.75. Sapphire is attractive for high temperature application because it's known chemical resistance and a high melting point. Single crystal sapphire fiber is transparent for transmission of visible and infrared light with small attenuation. The intrinsic loss of typical sapphire fiber is 0.13dB/m at the wavelength of 2.94 μm. With a high melting point, a sapphire fiber has the potential of delivering high optical energies larger than 1J/ pulse [5]. Because the Young's modulus of sapphire is 345GPa while that

of glass is around 60 to 90 GPa [6], a sapphire fiber is fairly stiff compared with a glass fiber. The minimum bend radius is ~45mm for a 300μm diameter sapphire fiber, while the standard glass fiber has a minimum bend radius less than 25mm [7].

A typical sapphire fiber has a hexagonal crystal structure as shown in Figure1.3 [8]. There are two principal optical axes inside a sapphire fiber, commonly referred to as the A-axis and C-axis, respectively. The C-axis is along the longitudinal direction of the fiber. The refractive indices along two axes are denoted by n_0 for C-axis and n_e for A-axis. As sapphire is a uniaxial crystal, the light with linear polarizations parallel and perpendicular to the C-axis (optical axis) has unequal indices of refraction [9, 10]. The typical birefringence magnitude of sapphire is about 0.008 as shown in Table 1.1[11].

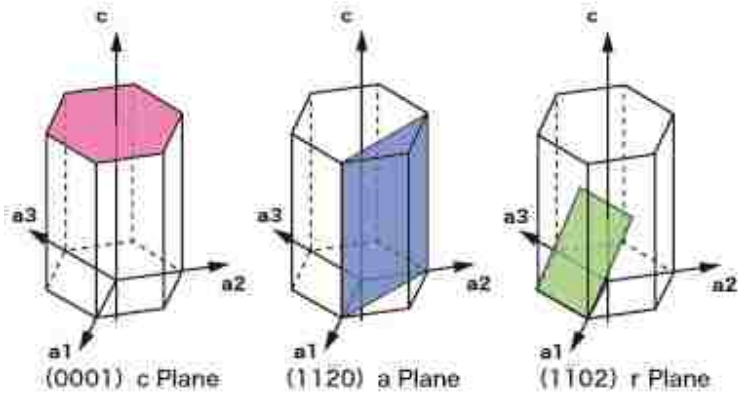

Figure 1.3. Sapphire crystal structure

There are currently two techniques for growing single crystal sapphire fibers. One is the Laser Heated Pedestal Growth (LHPG) method, and the other is the Edge-Defined Film-Fed Growth (EFG) method. The LHPG method was first reported by Gasson and Cockayne and Haggerty et al [5]. LHPG is known for obtaining high-optical-quality sapphire fibers for optical applications [12-15]. The main advantages of the LHPG technique include the high pulling rates and the possibility of growing materials with

very high melting points because of no crucibles are required during growth, allowing single crystals to be grown with high purity and low stress. A schematic of the growth apparatus by using LHPG method is shown in Figure 1.4. [16]. A CO_2 laser beam is directed to the Al_2O_3 source rod, where the tip is liquefied as the beam of a CO_2 laser is focused on it. A seed crystal is inserted into the liquefied part and pulled up to form a molten zone extending from the source zone. As the molten zone never contacts with a crucible or a die, the purity of the fiber is mainly determined by the purity of the source rod. In order to get good optical quality, the surface of a sapphire fiber should be smooth and the diameter is uniform along fiber. The fluctuation in the diameter of a sapphire fiber depends on the variation in the power of the CO_2 laser. A computer controlled feedback system can be used to stabilize the laser, as well as to control the fiber diameter. With this method, a sapphire fiber with diameter variation less than 0.5 % can be fabricated.

Table1.1. Refractive index of sapphire fiber

Microns	No	Ne
0.442	1.78038	1.77206
0.458	1.77843	1.77015
0.488	1.7753	1.76711
0.515	1.77304	1.76486
0.532	1.7717	1.76355
0.755	1.76141	1.75346
0.78	1.76068	1.75274
0.8	1.76013	1.7522
0.82	1.75961	1.75168
0.85212	1.75885	
0.8944	1.757	
0.98	1.75607	1.74819
1.0139	1.755	
1.064	1.75449	1.74663
1.12866	1.75339	
1.32	1.75009	1.74227
1.52952	1.74660	
1.55	1.74618	1.73838

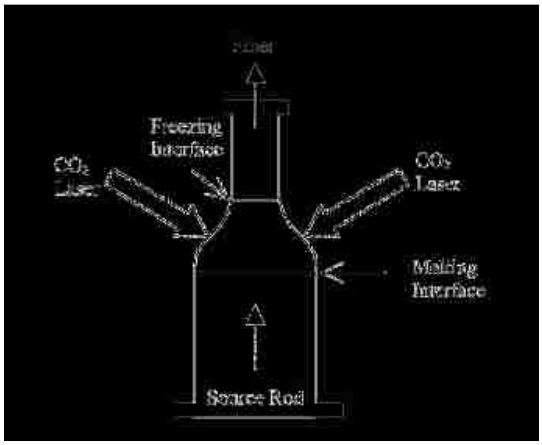

Figure 1.4. The laser Heated Pedestal Growth Process for growing single crystal sapphire fibers.

Edge-Defined Film-Fed Growth (EFG) is invited by Saphikon Incorporated [5].This method allows many sapphire fibers to be produced simultaneously, which makes the commercial production of sapphire fiber economically viable. As illustrated in Figure. 1.5.[8] , the EFG method needs a reservoir to contain the molten source material, which is used to continuously supply the growth of sapphire fiber. As the melt material is contained in a molybdenum crucible, the grown sapphire crystal will have 5 parts per million of molybdenum.

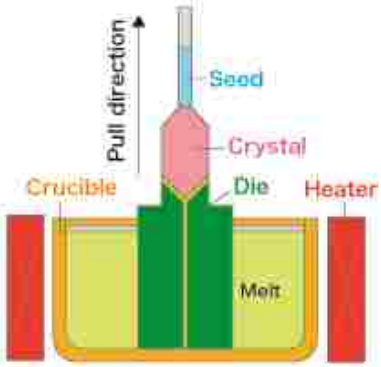

Figure 1.5. Schematic of using EFG method to grow sapphire fiber

2. COATING MATERIAL DEVELOPMENT AND NA MEASUREMENT

Sapphire fiber is very attractive for high temperature application. However, it has a much larger optical loss compared with glass fibers because the sapphire fiber surface cannot be as smooth as that of a glass fiber. In addition, it is currently difficult to manufacture low-cost fibers with perfect crystalline structure and uniform diameter [5, 17-19]. Also, a sapphire fiber cannot be grown in core-clad structures from rod-in tube source rods, as the molten zone contains rapidly moving convective flow patterns [20]. The geometry of rod-in-tube source rods will be lost once the source rods are melted. The un-cladded structure will lead to a large scattering loss along the rough sapphire fiber surface [19]. The un-cladded sapphire fibers also impose a number of undesirable characteristics for sensing applications, e.g., unpredictable light loss and highly multimode operation.

In order to improve the waveguiding properties and reduce unpredictable losses of a sapphire fiber, the Photonics Technology Laboratory (PTL) at Missouri S&T has collaborated with Prof. Dong's group at the University of Cincinnati to investigate the proper cladding materials for sapphire fibers. A stable cladding with appropriate optical and chemical properties can separate the core from the environmental contaminates to reduce the unpredictable scattering loss. The cladding also helps reducing the number of supported high-order modes in a sapphire fiber and the numerical aperture (NA) of waveguide.

This chapter begins with some fundamental introductions of sapphire fiber coating techniques and then describes our research processes on cladding material identification, development and characterization.

2.1. COATING TECHNIQUES FOR SAPPHIRE FIBER

2.1.1. Requirements of Cladding Material for Sapphire Fiber. Identification of suitable materials for cladding a sapphire fiber is difficult, because a number of requirements must be met simultaneously [18, 21]. An ideal cladding should enhance the optical waveguide properties and augment the mechanical and chemical strength of sapphire fiber. The cladding materials should 1) have a refractive index smaller than that

of sapphire, 2) be capable of operation over at least the same temperature range as sapphire, 3) possess a coefficient of thermal expansion (CTE) compatible with that of sapphire, 4) be able to form a strong bond between the cladding and the sapphire fiber, and 5) be dense and stress free in order to survive large fluctuations in temperature.

Many materials satisfy the index profile requirements. However, the materials that are thermally stable and stress-free in high temperatures are not easy to found. For a cladding material, the chemical reaction between cladding film and sapphire is not desired, and the diffusion of the cladding material into the sapphire is also prohibited. Film stresses are also needed to be considered, because they can cause a number of problems in high temperatures. The stress can divided into tensile stress and compressive stress, according to the direction of force along the fiber surface. Tensile stress could cause film cracking, while compressive stress could lead the film to buckle. The total stress can be expressed as a sum of thermal stress, intrinsic stress and extrinsic stress. Thermal stresses are primarily due to the differences in coefficients of thermal expansion of sapphire and coating material. Intrinsic stress, which is also called growth stress, is primarily generated by high energy configuration atoms or ions in the deposited film. Extrinsic stresses are produced from material phase changes or the interactions with the ambient. The conclusion is that the cladding must be a thermodynamically compatible film, preferably having a slightly lower thermal expansion coefficient than that of sapphire.

2.1.2. The Novel Double-Cladding Concept. As mentioned before, it is very difficult to find a single-component coating material that satisfies all the requirements described in Section 2.1.1 simultaneously. Therefore, a novel double-cladding structure is proposed to enhance the performance of sapphire fibers. As illustrated in Figure 2.1. , the cladding has two layers: an inner coating with a refractive index of n_1 and an outer coating of n_2. Although the refractive indices of the inner coating may be larger than that of sapphire, the refractive index of the outer coating is lower than that of the sapphire ($n_1 > n_0 > n_2$) so that total internal reflection condition is held at the interface between these two coatings. The propagating light is no longer guided by the sapphire-coating interface. Instead, the light is now guided by the inner-outer layer interface. The double-cladding concept presents an effectively approach to circumvent the challenging problem of

finding a single-component coating material that satisfies all the requirements. Instead, a matrix of coating materials can be designed to provide suitable optical, thermal and chemical properties. For example, we can now focus on the thermal and chemical properties of the inner coating material while design the outer coating material with proper thermal and optical properties.

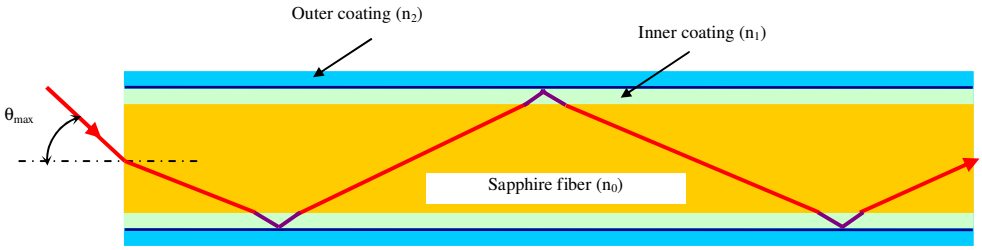

Figure 2.1. Illustration of differential double-cladding for sapphire fiber modification

2.1.3. Identification of Cladding Materials for Sapphire Fiber. The research of coating is mainly focused on two groups of candidate materials for the low index ($n_1<n_0$) outer coating and high index ($n_2>n_0$) inner coating, respectively. The low index materials will include MgO and aluminum oxide (Al_2O_3) and magnesium oxide (MgO)-based solid solutions because of their high melting temperature, high chemical and thermal stabilities, and low extinction coefficients. Some important properties for the candidate materials are listed in the Table 2.1 and Table 2.2.

Table 2.1. Properties for several candidate cladding materials

Material	Melting Point (^oC)	Boiling Point (^oC)	CET (10^{-6} K^{-1})
MgO	2850[22]	----	13.6[23]
Al_2O_3	2050[22]	2980[22]	6[24]
$MgAl_2O_4$	2135[22]	----	8.5
CeO_2	2600	---	10[25]

Table 2.2.Refractive indices for $MgAl_2O_3$ and $MgAl_2O_4$ at different wavelength

Wavelength (μm)	1.500	1.52952	1.55	1.6932	1.7092	1.8130	1.97009
n(MgO)	1.7153[26]	1.71496[27]	1.7147[28]	1.71281[27]	1.71258[29]	1.71108[29]	1.70885[30]
Wavelength (μm)	1.550	1.771	----	----	----	----	----
n (Al_2O_3)[31]	1.746	1.742	----	----	----	----	----
Wavelength (μm)	1.5152	1.52958	1.5625	1.6129	1.6667	1.7241	1.7857
n ($MgAl_2O_4$)[32]	1.6940	1.69468	1.693	1.693	1.692	1.691	1.690

The high index material considered is ceria (CeO_2). Ceria has a refractive index of 1.65 ~ 1.95 in visible and near IR ranges with superior thermal durability and is commonly used as a chemical barrier/buffer layers to stabilize oxide interfaces at high temperatures. The CTE value of CeO_2 is smaller than sapphire by 3 – 6 times which poses a mismatch of thermal expansion upon large temperature variations. The inner films of high index is therefore to be made thin enough (<2μm) so that the film not the fiber forms boundary space under tensile stress until fully annealed/relaxed. The small enlargement of the boundary space in trans-film direction is not expected to affect the waveguide function.

Recently, Prof. Dong's group has successfully coated MgO nanofilms on sapphire fiber. Preliminary tests indicated that the MgO film kept good chemical stability after fired in 700 ^oC . However, the interface of MgO and sapphire became blurring and at 1400 ^oC because of inter-diffusion between two different materials. The surface smoothness of MgO film also degraded at high temperature as Figure 2.2 shows. The experiments on double cladding of sapphire fibers are currently under exploration at the University of Cincinnati.

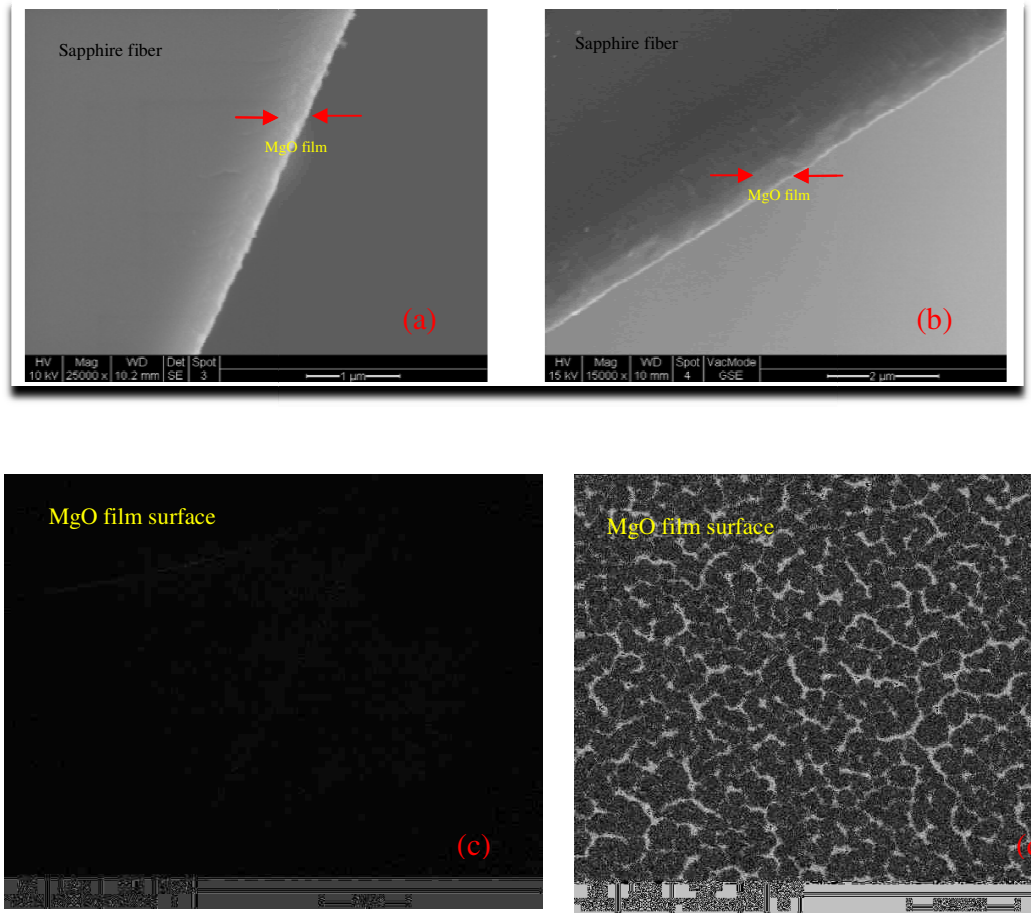

Figure 2.2 SEM images of MgO coated sapphire substrate. The substrate was fired at (a)(c) 700 ^{o}C and (b)(d) 1400 ^{o}C (Restults from University of Cincinati)

2.2. PRINCIPLES OF NUMERICAL APERTURE MEASUREMENT

2.2.1. Numerical Aperture Definition. The numerical aperture (NA) is an important parameter in an optical waveguide. Based on NA value, one can calculate the number of modes propagating within fiber. This value is directly related to the waveguiding ability and quality. The NA is defined as the sine of half the angle of the light acceptance cone of the optical fiber as shown in Figure 2.3. , and can be expressed by Equation 2.1:

$$NA = \frac{\sqrt{n_f^2 - n_c^2}}{n_0} = \sin\theta \qquad (2.1)$$

where n_c refers to the effective refractive index of cladding, n_f is the core effective refractive index and n_o is the refractive index of the ambient. As fiber is normally used in air, n_o equals to 1 if there is no other special declaration. θ is the half maximum incident angle of target fiber. Only the incident light with angle equal or smaller than θ can be trapped into the core of the fiber. Large NA value of fiber means more light can be trapped into the fiber core.

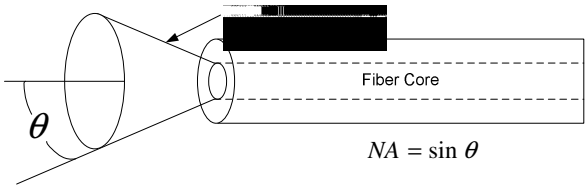

Figure 2.3. The schematic of light acceptance cone of an optical fiber.

2.2.2. NA Measurement Methods. From equation 2.1 we could know that if we can obtain the refractive index profile or the maximum acceptant angle of fiber, we can calculate the NA value directly. There are several approaches to measure the index profile and acceptant angle of an optical fiber, such as the transmitted near-field method, refracted near-field (RNF) method, and transverse offset method [33,34]. However, the most simple and commonly used technique for determination of NA value is to directly analyze the radiation pattern emitting from the fiber endface in the far field, which is called direct far field scan (DFF) method. There are two different arrangements to use the DFF method for NA measurement. One is using a camera to capture the power distribution from the fiber end and then using image process software to analyze the mode field patterns. The camera is placed on a linear stage so that its position relative to

the target fiber can be adjusted. The light acceptance angle of the fiber can be calculated by the mode field diameter changes in different positions. The accuracy of NA measurement using this method is limited by the low pixel resolution and potential power saturation of the camera.

Another experimental arrangement is mounting a photo detector on a rotation stage to catch the power distribution of the beam from the target fiber [34]. An optical source will overfill the input of the fiber, and the NA value is commonly calculated from the width where the intensity falls to 5% of the maximum of the output beam profile, given in Equation.2.2 [35]:

$$NA = \sin(\frac{\theta_1 + \theta_2}{2}) = \sin\theta \qquad (2.2)$$

where $\theta_1 + \theta_2$ is the total 5% intensity angle measured in DFF method as shown in Figure 2.4 [35].

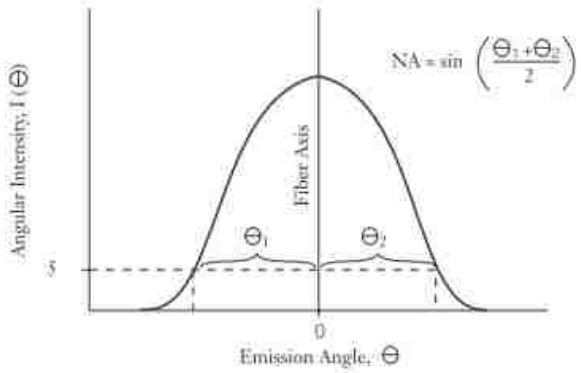

Figure 2.4 Direct Far-Field (DFF) method to measure the NA

The calculated value from Equation.2.1 is generally less than the measured value from Equation.2.2 due to the differential modes attenuation [36]. Also, the length of the measured fiber and excitation conditions are critical for NA measurement results.

In the following sections, the two DDF methods for NA measurement will be described in detail.

2.3. IDENTIFICATION OF CLADDING MATERIALS BY NA MEASUREMENT

2.3.1. NA Measurement System for Sapphire Plate. In order to identify the proper materials for cladding sapphire fibers, we built a system for measurement of the NA of sapphire waveguides. Sapphire plates are relatively cheap and easy to handle. As such, the cladding materials were first tried on sapphire plates. Correspondingly, a measurement system was established to measure the NA of coated and uncoated sapphire plates.

Before experiments, we have noticed that the endface of the sapphire plate is rough as shown in Figure 2.5 (a), the light impinges upon sapphire plate were scattered all round and scattering pattern suppressed the useful output pattern. The output pattern captured by IR camera was full of noise and hard to be analyzed. Therefore polishing of the sapphire endface was necessary before measurement. The polishing was performed using a wheel polisher (Ultrapol-1200, Ultra Tec) equipped with lapping film provided by Fiber Optical Center, and the rotation speed of polishing plate was about 40 rpm (rounds per minute). After 15 days of fine polishing, the endface of sapphire plate has been significantly smoothed as shown in Figure 2.5 (c).

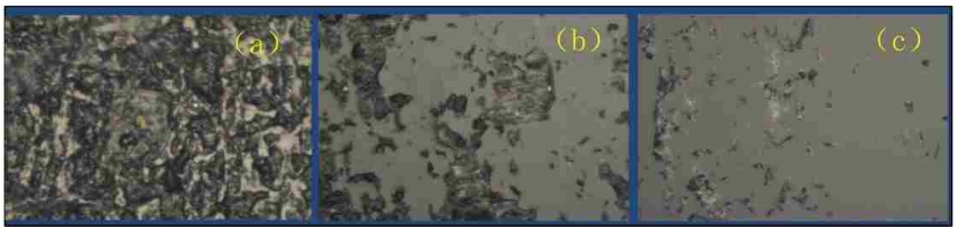

Figure 2.5. Polished sapphire end face. (a) The image of sapphire end face without polishing. (b) The image of sapphire endface after 8 days polishing. (c) The image of sapphire endface after 15days polishing.

In order to improve the polishing efficiency, the diamond lapping films (600X series) manufactured by 3M company was chosen to polish sapphire instead. The diamond lapping film was comprised of tightly grained diamond mineral which is uniformly coated on a polyester film backing. The hardness of diamond mineral was comparable with sapphire material, which could help to expedite the polishing. Two types of diamond lapping film were used: the sapphire plate was first polished using a lapping film with 3 μm grain size, and then fine polished using a lapping film of 0.1 grain size. By using the diamond lapping film, the whole polishing process could be completed in one day and the polishing results are showed in Figure 2.6.

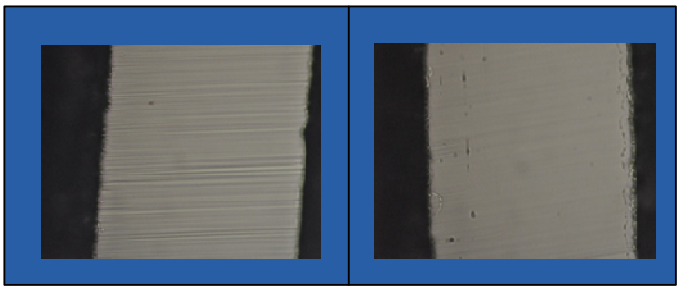

Figure 2.6. Diamond lapping film polished sapphire plate. Left figure is the image of sapphire plate polished by 3um grade diamond lapping film. Right figure is the image of sapphire plate after fine grinded by 0.1 grad diamond lapping film.

Because the lapping film has a pressure sensitive adhesive backing, it can be firmly fixed on the polishing plate. Therefore, we increased the rotation rate of polishing plate. However, to consider the firmness of the phenylsalicylate which is used to fix the polishing sample to the polisher holder, we limited the rotation rate below 80 rpm.

The NA measurement system is schematically shown in Figure.2.7.

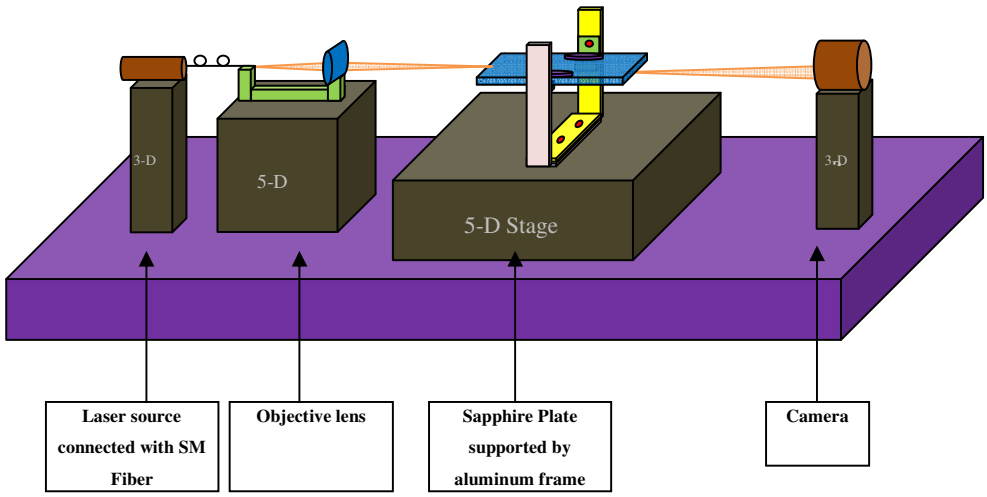

Figure 2.7. Experimental setup for measurement of NA of sapphire fiber plate.

A tunable laser emitting in the 1550 nm spectrum range (8164A, Agilent) was used as the light source. The light from the laser was first directed into the communication single-mode fiber through a standard FC connector. And then, the laser was focused into the sapphire plate through an objective lens (OFR LMO-10X-NIR) with a NA of 0.3. The output power distribution was captured by an InGaAs NIR Camera (SU320M-1.7RT, SENSORS UNLIMITED INC). The received pattern analyzed to calculate the acceptance angle θ and thus the NA value, according to the Equation.2.1.

The measurement principle is illustrated in Figure 2.8. The NRI camera is moved from one position to another with a step of ΔL, and the difference in the mode field diameter of output pattern captured in the two positions is Δh. Then θ_{max} showed can be obtained from the equation: $\theta_{max} = \arctan(\frac{\Delta h}{\Delta L})$.

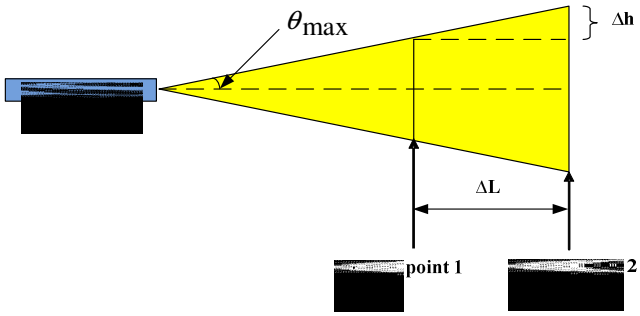

Figure 2.8. Schematic diagram of calculating NA value. The camera is moved from point 1 to point 2 to capture the output pattern at different positions.

The refractive index of sapphire at 1550 nm wavelength is about 1.745. The calculated NA value is 1.43. Considering the physical significance of NA, the maximum acceptance angle of sapphire plate should be 90^{o}, which indicates that light of any angle can be trapped and propagates in the uncladded sapphire waveguide.

The measured NA value of sapphire plate was 0.184 based on our experimental system. This value is limited by the NA of objective lens (0.3) used to launch the incident light as well as the spot size focused on the sapphire plate. The thickness of sapphire plate was about 0.3mm. The number of supported modes is about 5557at 1550nm wavelength. These modes cannot be evenly excited. Even the high order modes have been excited; their energies will be much lower than that of the fundamental mode and hard to be detected by the camera. We can increase the power of incident light to enhance the excitation of the high order mode. However, the power intensity of low order modes will also be increased, leading to saturation of the camera sensing area. As a result, the measurement accuracy is limited when a camera is used.

The other factor that limits the measurement accuracy is imposed by the size of camera focal plane. The camera has a focal plane array composed by 320×240 pixels, and the pixel pitch is 40μm. The total size of sensing area is about 1.28cm×0.98cm. In order to capture an output beam with a large divergence angle from the sapphire plate, the distance between the camera and sapphire plate end needs to be as short as possible. However, according to Equation.2.1., the NA value for an uncoated sapphire plate is

large than 1, that means the maxim emergent angle is 90 degree. It is impossible to use a camera to capture such a divergent light beam.

Based on the above reasons, it is not suitable to use a camera to perform the NA measurement of waveguide with large acceptance angle, such as sapphire fiber. Therefore, in the following sections, we will focus on using a photodetector as the measurement tool.

2.3.2. NA Measurement System for Sapphire Fiber. In order to overcome the above disadvantages of the former measurement system, a new test system based on the far field method has been constructed. In this system, the power distribution of sapphire waveguide is measured by scanning a fiber probe to acquire the output beam pattern point by point. The fiber probe can detect power along the meridian plane of sapphire waveguide. The sapphire fiber will be used as the sample target in the following sections. The polishing process of sapphire fiber is necessary, as the roughness of waveguide endface is a critical factor for the measurement accuracy.

2.3.2.1 The polishing process of sapphire fiber. The sapphire fiber used in our lab is purchased from Micromaterials and has a refractive index of ~1.75. As the hardness of sapphire fiber is 9 on the Mohs scale while common glass is 5.5, the sapphire fiber cannot be cut by common fiber cleaver. In order to obtain a smooth endface, the sapphire fiber is processed by using a polisher (Ultrapol-1200, Ultra Tec) equipped with diamond lapping films (668x-0.1μm, 3M).

The polishing process of sapphire fiber is similar with that of sapphire plate. The only thing need to be taken care of is that the sapphire fiber is much more fragile than the sapphire plate. As the sapphire fiber has a diameter of ~70 μm, the rotation speed of polishing plate needs to be small (less than 40 rpm) to avoid breaking the fiber.
The wheel polisher is shown in Figure 2.9. The sapphire fiber is clamped by a fiber adaptor. Compared with the previous method described in Section 2.3.1, the fiber adaptor can protect the coating layer of sapphire fiber because no glue will touch and contaminate the fiber coatings.

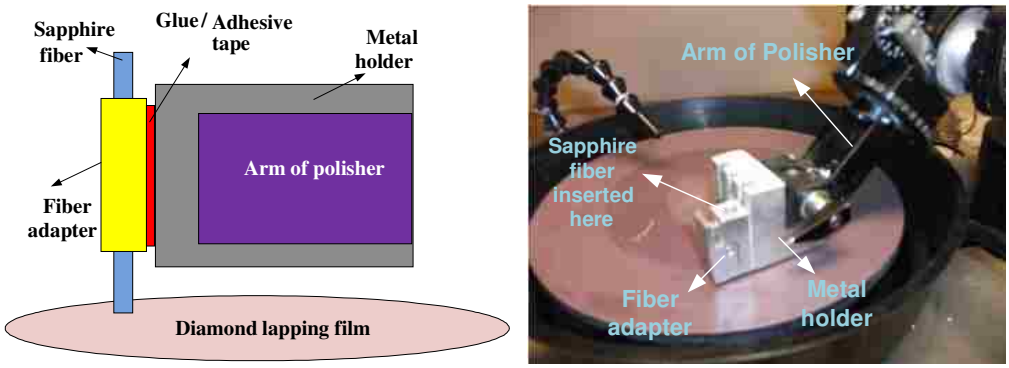

Figure 2.9. Polishing process setup. The left figure is the schematic drawing of polishing setup. The right one is the image of real experiment arrangement.

The following are the detailed procedures for polishing sapphire fibers:

a. Use the double-sided tape to attach the adaptor to the metal block as shown in Figure 2.9.

b. Insert the sapphire fiber into the adaptor.

c. Mount the metal block on the polisher. Use the gauge to adjust the position and make sure the end face of the sapphire fiber is parallel to the polishing plate.

d. Turn on the main power of polisher, and then keep the water flowing to protect the lapping film.

e. Accelerate the polishing plate slowly. The speed of rotation is set below 40rpm as the sapphire fiber is easy to break if the speed is too high.

When a sapphire fiber is broken, there is usually a long tip with a sharp edge remained at the end. It will be difficult and time consuming to obtain a complete endface by polishing only, for its hardness. As shown in Figure 2.10. (c), after several hours' polishing, the damaged part still could not be completely removed. To improve the efficiency, a femtosecond laser was used to cut the damaged part before polishing as illustrated in Figure 2.10. (a,b,d).

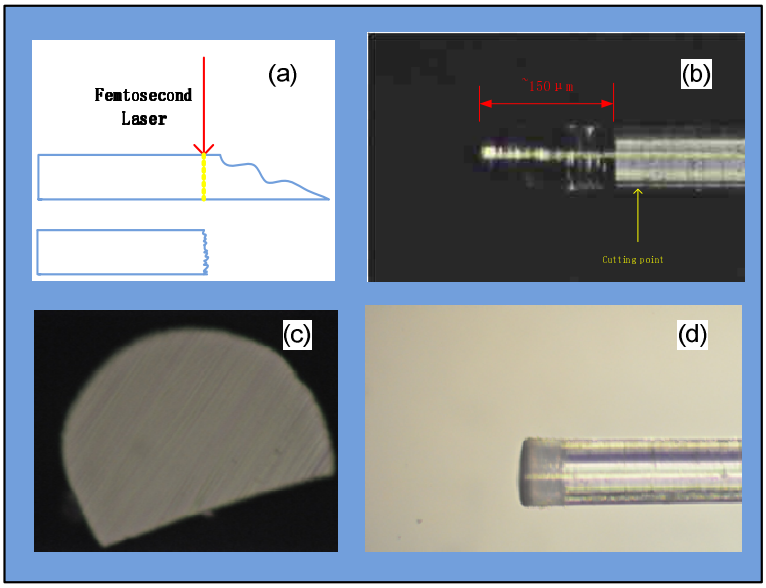

Figure 2.10. Laser cut and polishing of fiber end. (a) Schematic diagram of femtosecond laser cutting process. (b) Microscopic image of a sapphire fiber with damaged end. (c) Polihsed end face without cutting by a femtosecond laser (d) Microscopic image of a sapphire fiber cut by a femtosecond laser where the damaged part has been completely removed.

After cutting the damaged part, the end face of the sapphire fiber was flat. However, as shown in Figure 2.11 (a, b), the surface was rough. This rough surface diffracts the light and produces an error in NA measurement. To obtain a smooth endface, a 3μm diamond lapping film was used to polish the pre-processed fiber. The microscopic images of the polished endface are shown in Figure 2.11 (b,e). There were some visible polishing traces that could be observed by microscope. A lapping film with 0.1μm grain size was used to fine-polish the sapphire fiber end face, and the result is shown in Figure.2.11(c, f).

It is worth noting that the shape of sapphire fiber end face is hexagonal instead of round, which is much different from the glass fiber. This is because the sapphire is made of mono-crystalline material, while the glass fiber is made from amorphous forms' silica.

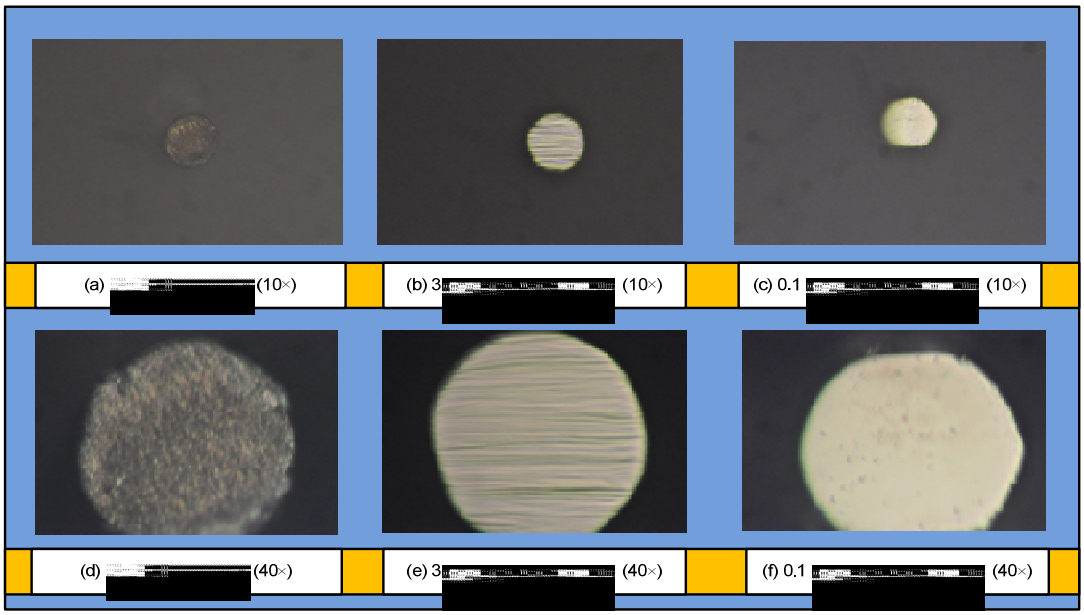

Figure 2.11. Microscopic images of sapphire fiber endface. Endface image after (a, d) femtosecond laser cutting, (b, e) polished using a 3µm diamond lapping film, and (c, f) polished using a 0.1µm diamond lapping film.

Figure 2.12 shows the side images of a sapphire fiber after femtosecond laser cutting and polishing. The small sapphire particles generated from cutting process surround the fiber tip, appear as the black shadow around the fiber end as shown in Figure.2.12. (a). These particles have been removed after polishing as shown in Figure.2.12. (b).

2.3.2.2 NA measurement system for sapphire fiber and experimental results.

The schematic of the NA measurement system is shown in Figure 2.13. The system consists of an iris diaphragm, a 20X magnification objective, a photodetector, a number of high quality precision stages, blocks, and fiber holders. Fiber samples are aligned through two fiber holders, which are fixed on a 3-D stage with resolution of 1µm. All the optical components have been centrally aligned with the help of a visible red laser from the Visual Fault Finder (FFL-050, JDSU).

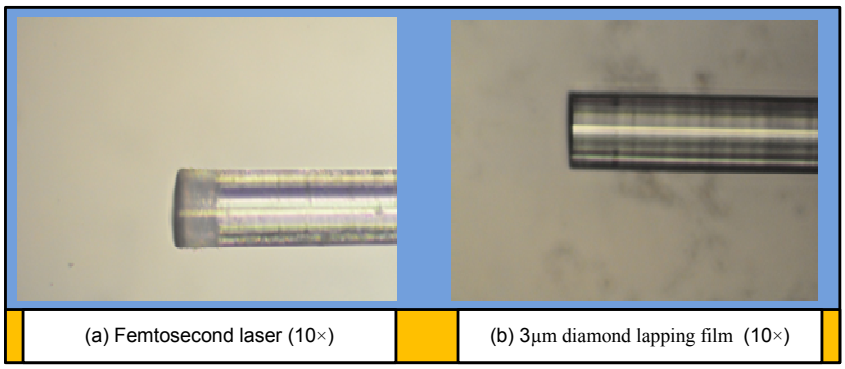

Figure 2.12. Sapphire fiber end face after laser cutting and polishing. (a) Side image of a sapphire fiber cut by a femtosecond laser. The endface is surrounded with small sapphire particles generated from cutting process. (b) Microscopic image of a sapphire fiber fine-polished after femtosecond laser cutting.

A high power semiconductor laser emitting at the wavelength of 980nm was used as the light source. The light from the laser was launched into a 70m-long multimode fiber (MMF, Infinicor 600, Corning). The fiber was chosen long enough so that all the guided modes were evenly excited. To strip the cladding modes of MMF, a small section of MMF was coiled with a diameter of about 1cm. The MMF had an NA of 0.2 producing an output light beam with a maximal divergence angle of 22 degree. The light beam from the MMF was then focused into the measured fiber through a 20× objective lens with maximal numerical value of 0.43 (maximal angular aperture is 53^{o}) and focal length of ~9 mm. The iris diaphragm placed between the graded index multi-mode fiber and objective is used to continuously control the incident light allowed into the measured sapphire fiber. The photodetector is placed about 2.5 cm away from the sapphire fiber end, and fixed on a rotation stage with 1nm resolution. Each time, we manually rotate the rotation stage with a step of 1 degree to obtain the power intensity at that direction. Basically, 90 sample points are enough to display the power distribution of tested fiber.

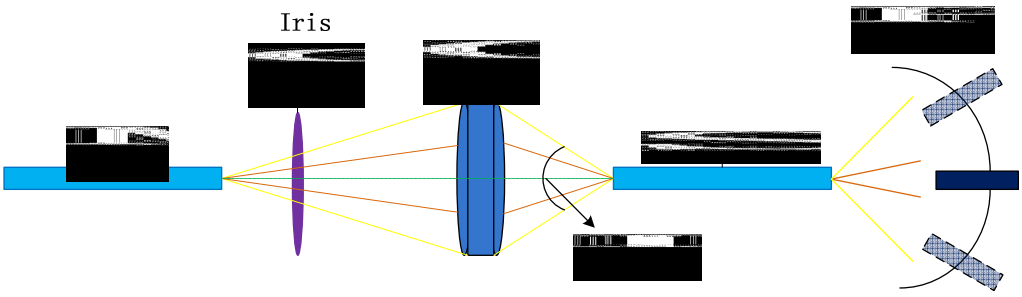

Figure 2.13. The experimental arrangement of sapphire fiber numerical value measurement

The sapphire fiber that we tested in our experiments includes two different types: one is coated with MgO and the other is uncoated. The refractive index of MgO is about 1.7147 at the wavelength of 1.5 μm. Therefore the theoretical NA value of a MgO coated sapphire fiber should be 0.35 according to Equation 2.1. The sapphire fiber was tested by using the system shown in Figure 2.13. The output power distributions of the coated and uncoated fibers are shown in Figure 2.14. The length the test fibers was about 10cm. The power distribution curves of the coated fiber are obviously smoother and narrower than the uncoated ones under the same measurement condition. This is because the coating material has helped reduce the number of supported modes.

The calculated NA results are shown in Table 2.3. When the NA value (13 dB) of incident light is 0.36, the measured NA value (13 dB bandwidth) of the coated sapphire fiber is around 0.14, which is smaller than the measured NA value of 0.19 obtained from the uncoated sapphire fiber. Compared with the theoretical NA value of 0.35, the measured result of cladded sapphire fiber is much smaller. This is probably because the NA value of incident light is only 0.36 and cannot excite all supported modes in sapphire waveguide. However, based on the test results, it is still manifest that this material is useful to improve the optical prosperities of sapphire fiber.

Sapphire fiber without coating	Sapphire fiber with coating (MgO)
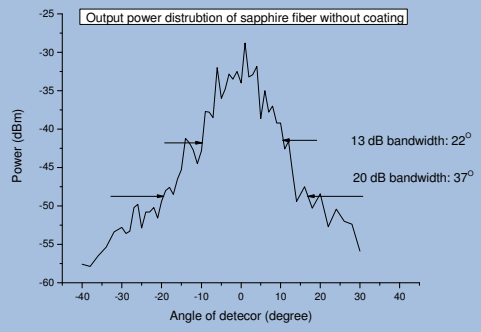 Incident angle: 42.24°	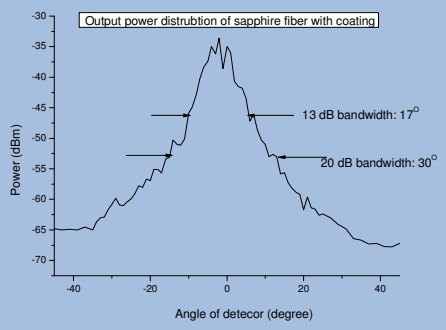 Incident angle: 42.24°
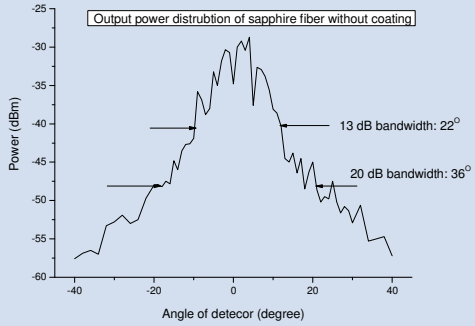 Incident angle: 27.45°	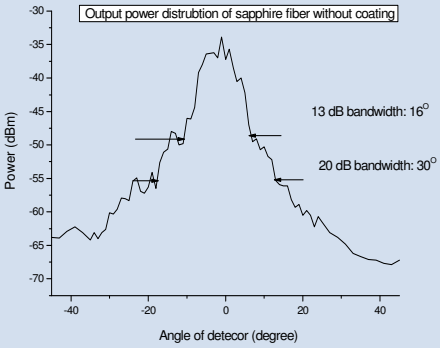 Incident angle: 27.45°
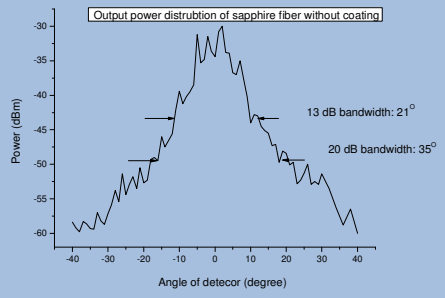 Incident angle:9.96°	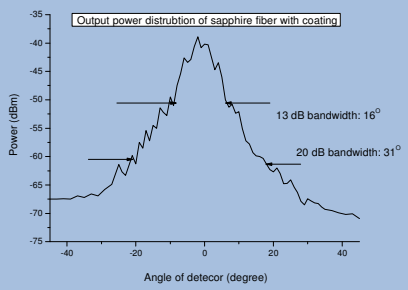 Incident angle:9.96°

Figure 2.14. Sapphire fiber NA measurement with/without cladding layer

Table 2.3. Measured NA values of coated and uncoated sapphire fiber

Incident NA	Measured NA of uncoated sapphire	Measured NA of coated sapphire
0.36	0.19	0.15
0.24	0.19	0.14
0.09	0.18	0.14

2.3.2.3 Automation of NA measurement system. The resolution of manual rotation stage described in the last section is one degree. The low resolution limited the accuracy of measurement. In addition, the output beam angle from an uncoated sapphire fiber can be as large as 90°. Manually rotating the stage and input data is not only slow but also increases the chance of error due to instability of the laser power and measurement setup. In this section, we describe an automated measurement system which utilizes a motorized stage with high resolution. The motorized stage was purchased from Tholarb (CR1-Z7) which provide a 5-arcmin angular resolution. In our experiments, we used an increment step of 0.1 degree.

A Labview program has been written to control the motorized stage and power detector for automated NA measurement. The user graphic interface and the block diagram of the control program shown in Figure 2.15.

The experimental setup for NA measurement has been slightly modified to have two objective lenses as shown in Figure 2.16. In the modified system, an objective lens was used to replace the original iris diaphragm. The first objective lens was to collimate the beam exiting from the input fiber. The second objective lens was used to focus the beam into the sapphire fiber. The pair of objectives not only saved the incident power but also allowed a larger excitation angle. The NA values of the first and second objectives were 0.14 (10×) and 0.86 (50×), respectively. The picture of the automated NA measurement system is shown in Figure 2.17.

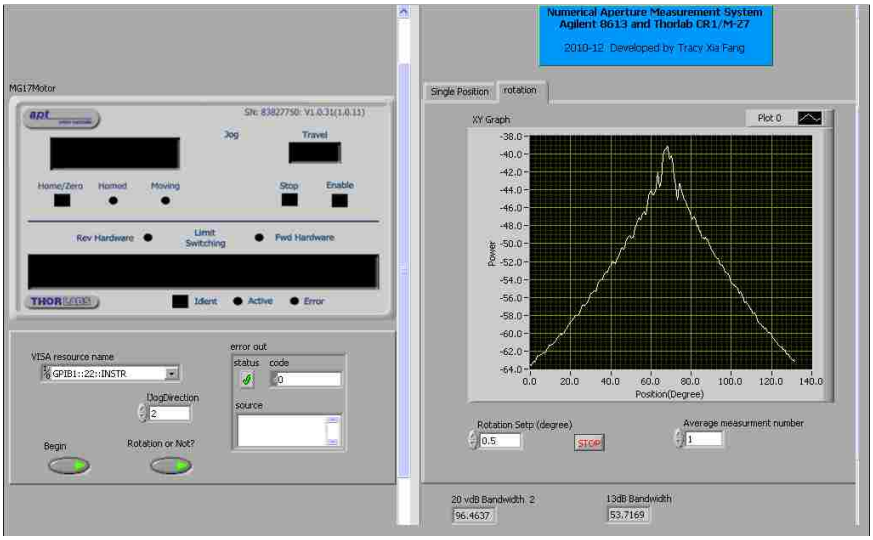

(a)

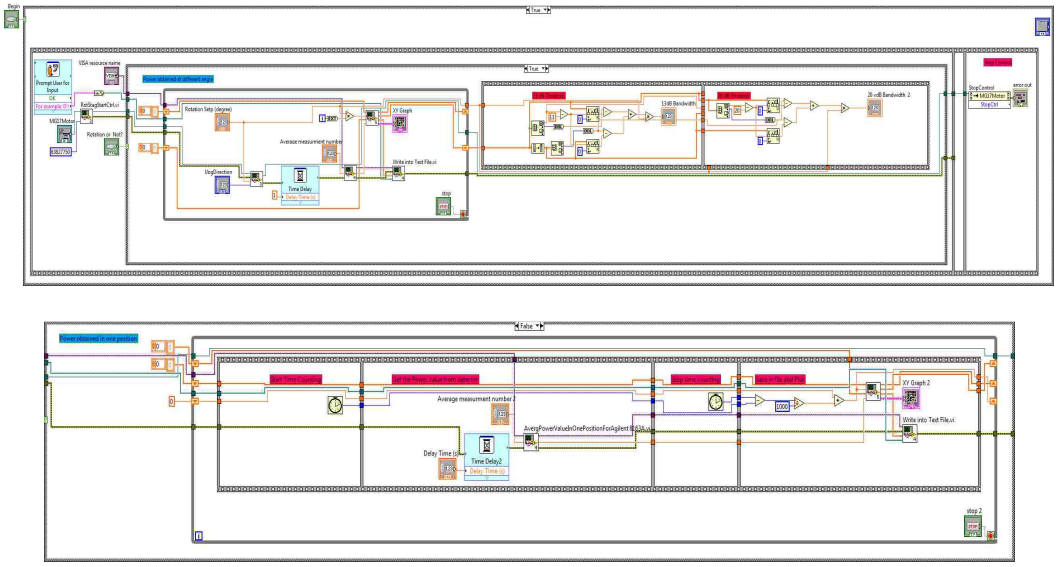

(b)

Figure 2.15. LabView program for the NA measurement system. (a) User graphic interface of the program, (b) Block diagram of the program.

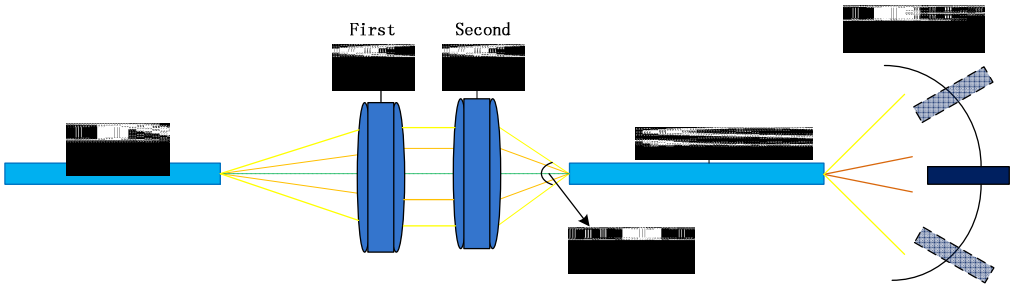

Figure 2.16. Schematic of the optical system for sapphire fiber NA measurement system

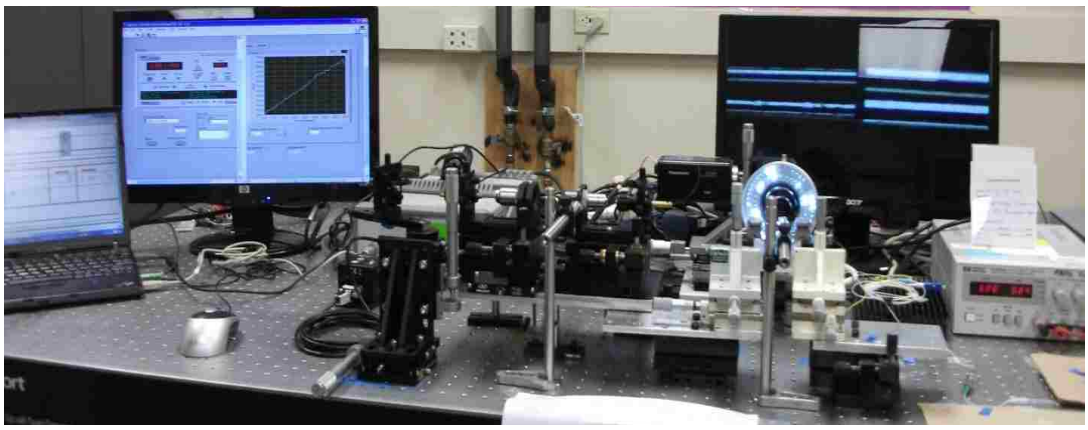

Figure 2.17. Photograph of the automated NA measurement system

Figure 2.18 shows the output power distributions of an uncoated and a coated sapphire fiber. The measured NA values of the two sapphire fibers are listed in Table 2.4. The cladded sapphire fiber was overfilled by the focused beam from the 50× objective lens. The NA of the cladded sapphire fiber was measured to be 0.39 which was slightly larger than the theoretical value of 0.35, but was significantly smaller than the excitation NA of 0.86 .The probable reason is that there are still a lot of unstable modes existing as the length of coated fiber is only 10 cm long. These unstable modes cannot be completely stripped out in this short length sapphire fiber. The 10cm cladded sapphire fiber has taken over 3 months to coat in our current experiment condition. With consideration of cost and

time consumptions, the longest acceptable length of test sapphire is only10cm. The measured NA value for uncoated sapphire fiber is about 0.52 which is much less than theory value of 1. That is because in practice, uncoated sapphire fiber surface is uneven and scatters the light into large-angle lossy modes. The effective NA of uncoated sapphire fiber is commonly much less than the theoretical value. Actually, the effective numerical aperture of fiber provided by Micromaterials is only 0.45 for the 300 μm diameter sapphire fiber of 1 meter long.

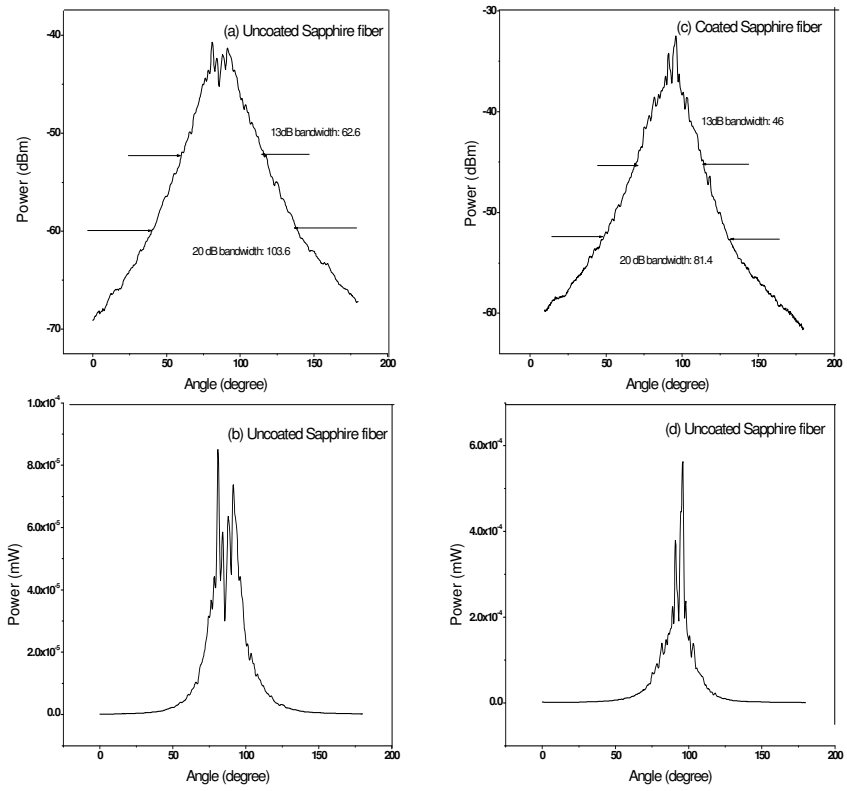

Figure 2.18. Power distribution of coated and uncoated sapphire fiber. (a) The output power distribution of uncoated sapphire fiber in dB scale and (b) in linear scale. (c) The output power distribution of coated sapphire fiber in dB scale and (d) in linear scale.

Table 2.4. Measured NA values of coated and uncoated sapphire fiber

Incident NA	Measured NA for coated sapphire	Measured NA for uncoated sapphire
0.86	0.39	0.52

3. FABRICATION AND HIGH TEMPERATURE EVALUATION OF SAPPHIRE FIBER SENSOR

Over the past several decades, fiber optic sensor technology [37, 38] has been widely investigated for their proven advantages of compact size, immunity to electromagnetic interference and resistance to adverse environments. Most fiber sensors such as those based on fiber Bragg gratings (FBG) and Fabry-Perot interferometers are fabricated in conventional silica-based fibers. These silica fiber based sensors cannot be used in harsh environments with a temperature over 1150 ^{o}C [39, 40], due to the relatively low melting point of glass. In an effort to increase operating temperature of optical sensors, researchers have found that the sapphire fiber based sensor is one of the promising candidates due to the high melting point of about 2053 ^{O}C for sapphire fiber. Up to date, a number of sapphire fiber sensors have been reported such as sapphire fiber blackbody thermometers [41], extrinsic and intrinsic sapphire fiber Fabry-Perot interferometers (FPI) [42]. Some sapphire-based sensors have been proven to be operational in temperature up to 1600 ^{o}C in laboratory. However, most of this kind of sensor need assembly components ,originated from their fabrication process [43]. As a result, the long term stability is a concern.

In this chapter, an assembly-free sapphire fiber based hybrid extrinsic/intrinsic Fabry-Perot interferometer (HEIFPI) fabricated by femtosecond laser micromachining technology will be demonstrated. As there are no additional components needed to support alignment or packaging, the operational temperature can be increased to 1560^{o}C.

3.1. PRINCIPLE OF HEFPI SAPPHIRE FIBER SENSOR

The principle of the sensor is schematically illustrated in Figure 3.1. A broadband source (e.g., an amplified spontaneous emission (ASE) source made of Erbium doped fibers (EDF) emitting in the conventional band (C-band: 1530-1565nm) and long band (L-band: 1565-1625nm)) is directed by a C+L band coupler, passing through a specially designed low loss singlemode-multimode-sapphire fiber splicer (SMS), to excite the HEIFPI probe placed in the high temperature zone. The HEIFPI generates a backward-propagating optical signal containing the information of local temperature and dynamic

pressure into an optical spectrum analyzer (OSA). The data are acquired and processed by a computer to produce the measurement results.

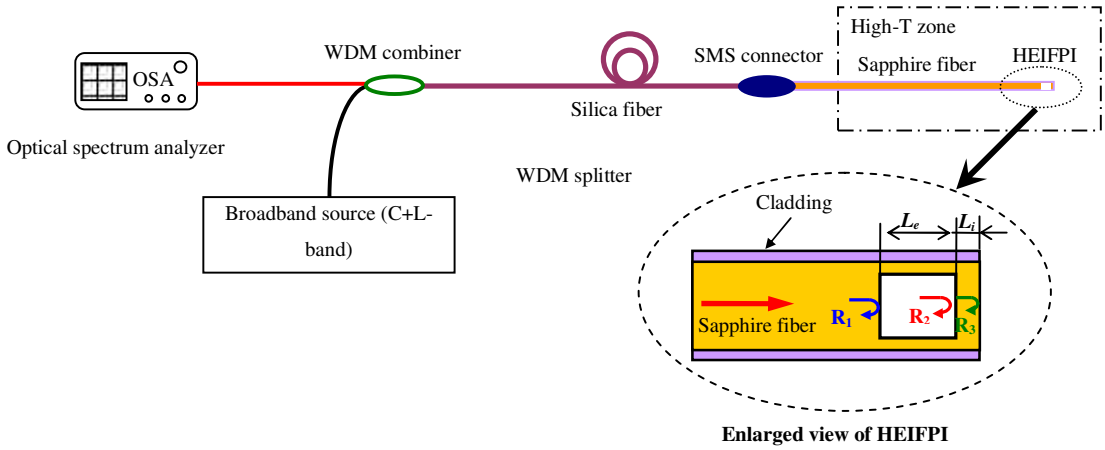

Figure 3.1. Operating principle of microstructured sapphire HEIFPI sensor for high temperature measurment

As shown in the enlarged view, the HEIPFI is fabricated as a microhole in the sapphire fiber by femtosecond laser ablations, leaving a thin, supported diaphragm at the sapphire fiber tip.

The incident light generates three reflections (R_1, R_2 and R_3) from the three endfaces (i.e., the two endfaces of the microhole and the endface of the sapphire fiber tip), respectively. These three reflections produce an interference signal when mixed at the detector. In this hybrid structure, two low finesse Fabry-Perot interferometers are formed. One is the air-gap extrinsic Fabry-Perot interferometer (EFPI) formed by the microhole (R_1 and R_2). The other is the intrinsic Fabry-Perot interferometer (IFPI) formed by the sapphire diaphragm (R_2 and R_3). The three-beam interference signal is given by:

$$I = I_0 \left\{ R_1 + R_2 + R_3 + 2\sqrt{R_1 R_2}\cos\left(\frac{4\pi}{\lambda} L_e\right) + 2\sqrt{R_2 R_3}\cos\left(\frac{4\pi}{\lambda} L_i n\right) + 2\sqrt{R_1 R_3}\cos\left[\frac{4\pi}{\lambda}(L_e + L_i n)\right] \right\} \tag{3.1}$$

Where, I_0 is the intensity of the incident light, L_e is the length of the microhole forming the EFPI, L_i is the thickness of the sapphire diaphragm forming the IFPI, n is the refractive index of the sapphire fiber, and λ is the optical wavelength in vacuum. Equation (3.1) indicates that there are three frequency components in the interference spectrum, corresponding to L_e, nL_i and their sum ($L_e + nL_i$), respectively.

If we ignore the reflection power R_3, we can simplify Equation (3.1) into:

$$I = I_0 \left\{ R_1 + R_2 + 2\sqrt{R_1 R_2}\cos\left(\frac{4\pi}{\lambda} L_e\right) \right\} \tag{3.2}$$

As the temperature changes, the cavity begin to expand or condense. The temperature information can be obtained by the length change of cavity (L_e) through analyzing the signal spectrum from OSA.

3.2. INVESTIGATION ON THE COUPLING BETWEEN GLASS LEAD-IN FIBER AND SAPPHIRE FIBER

One of the most critical issues associated with the microstructure sensor is the coupling between lead-in fiber and sapphire fiber (SF). Light coupling efficiency between lead-in fiber and sapphire fiber is associated with a number of parameters. Thus, it is almost impossible to study the coupling efficiency as a whole. In order to solve this problem, we decomposed the coupling into three relatively simple and straightforward sub-issues, and investigated these three sub-issues individually. The first sub-issue is **forward coupling efficiency**, which by definition, describes the coupling efficiency from lead-in fiber to SF. The second sub-issue is the **backward coupling efficiency**, which describes the coupling efficiency from the SF to lead-in fiber. And the third sub-issue is the **coupling interfaces resulted limitation**, which is the DC signal generated by the lead-in fiber interface and the SF interface.

3.2.1. Forward Coupling Efficiency. As shown in Figure 3.2, the lead-in fiber, which may be chosen from a range of different fiber types including single-mode fiber (SMF), graded-index multimode fiber (GIF) and step index multimode fiber, is sending

light wave to the FP structure via SF. Forward coupling efficiency (η_F) is defined as the power coupled into the SF over the power output from the lead-in fiber. In our sensing application, it is desired to have more power transferred to the FP structure. Therefore, in order to optimize the system, we need to maximize the forward coupling efficiency.

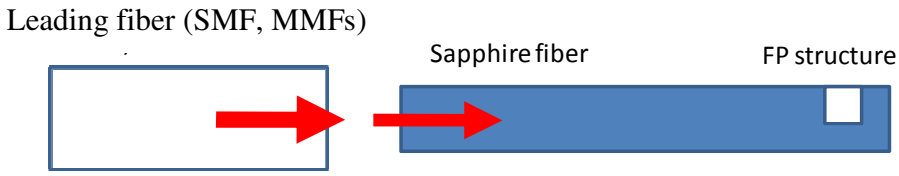

Figure 3.2. Forward coupling efficiency

The Forward coupling efficiency evaluation experiment arrangement is shown in Figure 3.3. A tunable laser (HP 8168F) was tuned at 1550 nm with a power of 3 mW. Light was directed through a single mode fiber (SMF) to lead-in fiber, and then sent into a double-side polished SF.A home-made fixture which could grip the sapphire fiber by only two touching points was used to hold the SF. The fixture can significantly reduce the surface contact area and keep light propagating in SF waveguide. A five-axis precision stage was used for mounting the fixture and a power meter (Agilent 81618A) was placed on the other side of the SF to measure the transmitted energy.

The experiment results show that the forward coupling efficiency is very close to 1 (zero in dB scale) with different lead-in fibers (SMF, and a set of different index multimode fibers). Only a little variation at a scale of 0.1 dB, and it is mainly contributed by fiber alignment mismatch. Also, with/without applying refractive index matching fluid would result in very similar forward coupling efficiency.

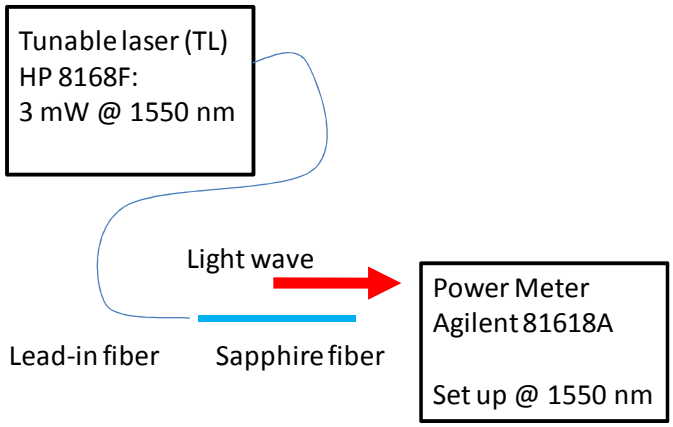

Figure 3.3. Experiment setup to evaluate forward coupling efficiency

From the experiment results, it is concluded that the forward coupling efficiency is very close to 1. It is neither a function of adhesive between SF and glass fiber, nor a function of lead-in glass fiber type. In other word, the forward coupling efficiency does not limit the coupling between SF and lead-in glass fiber. This is mainly because the sapphire fiber has much larger NA and core dimension than the lead-in fiber.

3.2.2. Backward Coupling Efficiency. Upon the interaction between input light wave and the FP structure, some of the light will be reflected from the interfaces inside, as shown in Figure 3.4. The reflection light carries the interferometric signal which can be interrogated by the equipment connected to the lead-in fiber. However, SF has a larger core size and NA than that of the SMF, which leads to the fact that only a small portion of light is able to be collected by the SMF lead-in fiber. The portion of light energy coupled into the lead-in fiber over the energy output from the SF is defined as backward coupling efficiency (η_B). For the purpose of making the return signal detectable, the energy collected by the lead-in fiber should be larger than the detection threshold of OSA. Therefore, a high backward coupling efficiency is preferred.

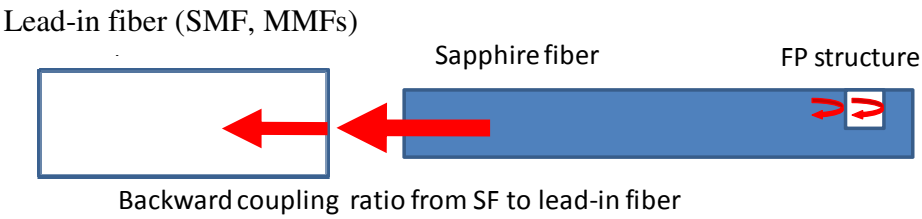

Figure 3.4. Schematic diagram of backward coupling efficiency

With the aim of improving the backward coupling efficiency, an evaluation experiment was designed and conducted, as shown in Figure 3.5. A group of lead-in fibers (SMF, MMF-GIF-50, MMF-GIF-60 and MMF-GIF-100) are evaluated respectively with/without applying index matching fluid and Norland optical adhesive (NOA).

The main idea of the backward coupling efficiency evaluation experiment is to excite the sapphire fiber from one side and collect the power on the other side using different lead-in fibers. By comparing the input and output laser power, we are able to calculate the backward coupling efficiency (η_B) referring to Equation. (3.2).

$$I_{input} = I_{output} \times \eta_B \tag{3.3}$$

or $$I_{input} = I_{output} + \eta_B \quad \text{in dB}$$

where I_{input} is the output power from the right side (adjacent to the tested lead-in fiber, as shown in Figure 3.5) of the SF, and I_{output} is the energy detected by the power meter connected to the lead-in fiber.

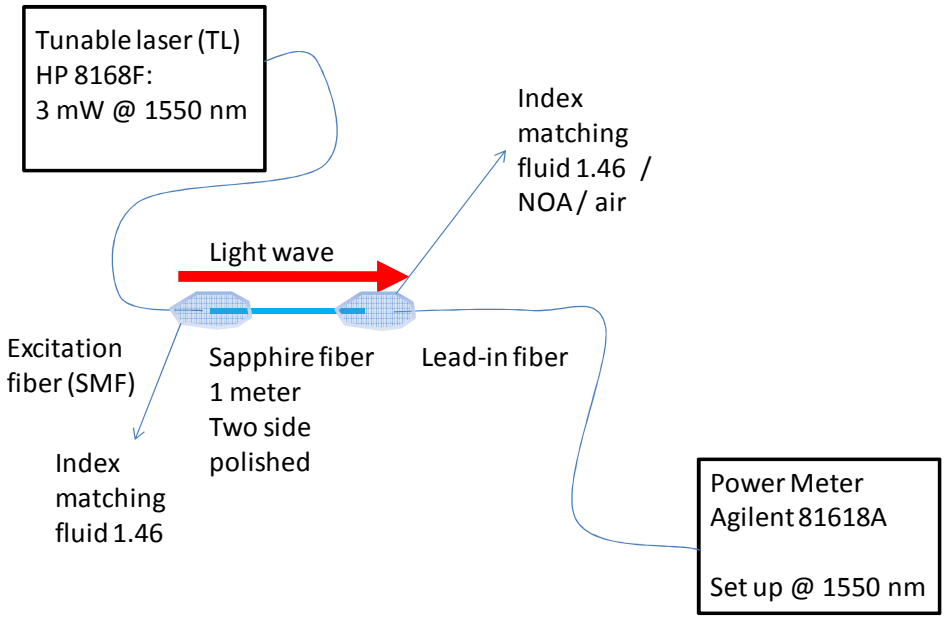

Figure 3.5. Backward coupling efficiency evaluation experiment setup

The length of SF used in experiment is 1m, with both sides machine polished. A single mode fiber is connected to the tunable laser (HP 8168F) to excite the SF. Also, a fusion splicer is used to align the excitation SMF and the SF.

The alignment between SF and the lead-in fiber was achieved by two sets of 5 axis stages. As shown in Figure 3.6. , one of the stages has the home-made two-points touching SF holder mounted on it and the other one has a general-purpose fiber holder fixed on it. A camera is used to monitor the fibers during the fiber alignment operation. A mirror in 45° is placed under the two fibers for the purpose of capturing the fiber images from both front-view and top-view to assistant the alignment process.

The measured backward coupling efficiencies with various lead-in fibers under different conditions are shown as Table 3.1.

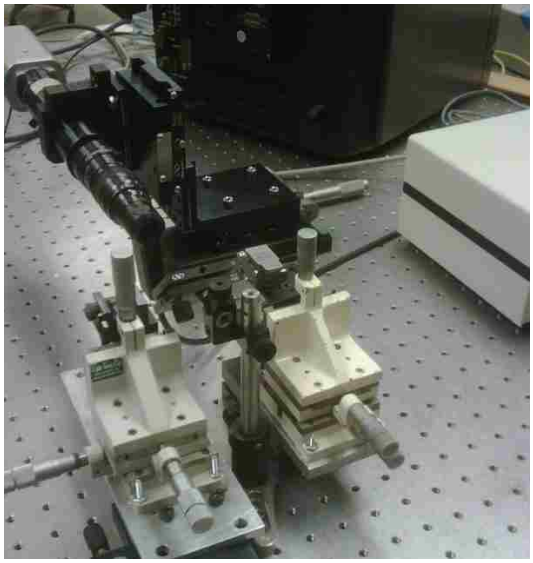

Figure 3.6. Picture of the backward coupling efficiency evaluation experiment

Table 3.1. Backward coupling efficiency with different lead-in fibers and adhesive

η_B \ Unit (dB)	Free space	Matching fluid	NOA
SMF	-14.40	-13.60	-14.40
GI MMF 50/125	-3.90	-3.48	-3.90
GI MMF62.5/125	-2.48	-2.20	-2.15
GI MMF100/140	-0.80	-0.34	-0.34

From the measurement results, it can be seen that the backward coupling efficiency is much lower than the forward coupling efficiency. The possible reason is that the dimension mismatch and numeric aperture difference between lead-in fiber and SF makes only a portion of light wave energy to be coupled back. As shown in Table 3.1, the SMF has the lowest backwards coupling efficiency of around -14 dB, while the 100/140 MMF has the highest efficiency of about 0dB. From the experiment results, it can be concluded that the MMF with larger core size can provide higher back coupling efficiency.

3.2.3. Coupling Interfaces Resulted Signal Limit. The connection between SF and the lead-in fiber forms two interfaces. They are the interface of lead-in fiber and adhesive (air/refractive index matching fluid/NOA), and the interface of SF and adhesive (air/refractive index matching fluid/NOA). Both interfaces may result in DC reflection signal in the reflection spectrum. If the FP structure signal is smaller than either of the two interface induced reflection power, the FP structure signal would be overwhelmed by the DC reflections. Correspondingly, the reduction of the interfaces reflecting power is essential to make the interferometric signal readable.

In this section, two differently processed sapphire fiber endfaces have been investigated. One sapphire fiber end is mechanically polished, and the other one is cut by femtosecond laser.

The evaluation experiment of interface reflection is illustrated in Figure 3.7. An ASE source power is directed into sapphire fiber via a C-band optical circulator. The port 2 is cut by femtosecond laser to minimize the reflection power. The port 3 of circulator is connected with an optical power detector (Agilent 81618A), which is used for real time monitoring the reflection power generated from the interfaces. Another power detector is put at the end of sapphire fiber to monitor the transmission light.

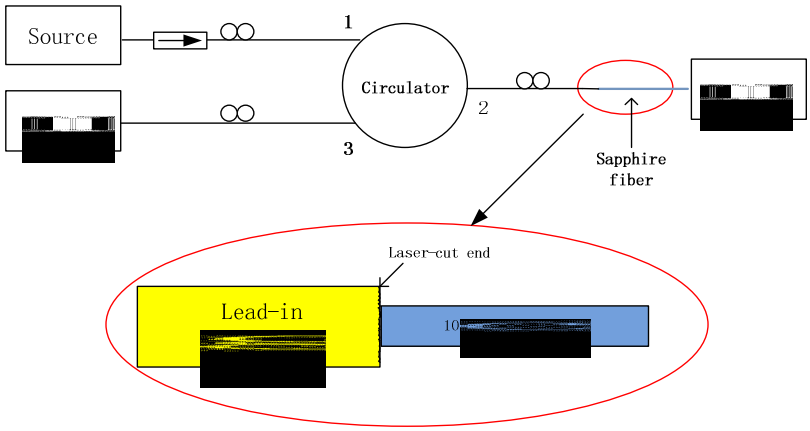

Figure 3.7. Experimental setup of interface reflection measurement

As mentioned in Section 2, the femtosecond laser processed sapphire fiber usually has an endface with roughness scale of several microns. This rough end can be helpful to reduce the interface reflection compared with the polished fiber end. In order to experimentally prove it, two different pre-processed sapphire fibers has been used as test samples: one has double polished ends and another has polished and laser cut end on each side.

First, the power from port 2 and 3 of the circulator in Figure 3.7 without butt connection to the sapphire fiber was measured. The only reflection interface is between port 2 glass fiber endface (GF) and surrounding air (GF/air interface). The transmission power at port 2 (lead-in fiber) is about -17.48dBm, and the reflection power collected from port 3 is about -52.73dBm. Then the double-side polished sapphire fiber was mechanically connected to the lead-in fiber in port 2 as shown in Figure 3.8. The reflection power collected in port 3 then increased to -43.20dBm, which was contributed by the GF/air/P1 interfaces and P2/air interface together as shown in Figure 3.8. P1 refers to the left polished side of sapphire fiber, and P2 refers to the right polished end. In order to figure out how much power can be reflected from P2 interface individually, P2 was put into 1.46 refractive index matching oil and the reflection power did not change very much as shown in Table 3.2 .That means the main contribution for the total reflection power is from GC/air/ P1, not the P2/air interfaces. The DC power from the connection point (GF/air/P1) has overwhelmed the possible signal power from sapphire end (P2). It is not desirable for sensor application and better connection methods need to be investigated for reducing the DC reflection power from connection point.

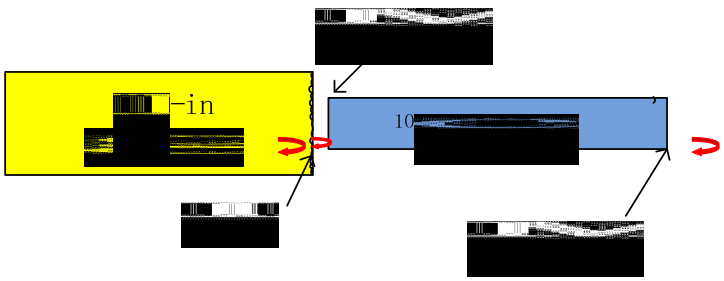

Figure 3.8. Laser cut SF endface without index matching fluid

Table 3.2 Reflection and Transmission Power of polished sapphire fiber connection

Polished sapphire end	GF/Air	GF/Air Air/P1 P2/Air	GF/Air Air/P1 P2/ matching oil (RI:1.46)
Reflection Power	-52.73dBm	-43.20dBm	-43.50dBm
Transmission power	-17.48dBm	-21.83dBm	Cannot be measured

To decrease the connection reflection, a laser-cut sapphire fiber is tested in the following experiment. The scheme of the connection is shown in Figure 3.9, and the test results can be found in Table 3.3. The laser-cut fiber end (C1) helped to reduce the reflection power from -43.20dBm to -51.77dBm, and the index matching oil in the connection point could further reduce the reflection power to -53.35dBm. In order to calculate how much energy is reflected from P2, the P2 endface was immersed into acetone and the reflection power was reduced to -59.42dBm as shown in Table 3.3.

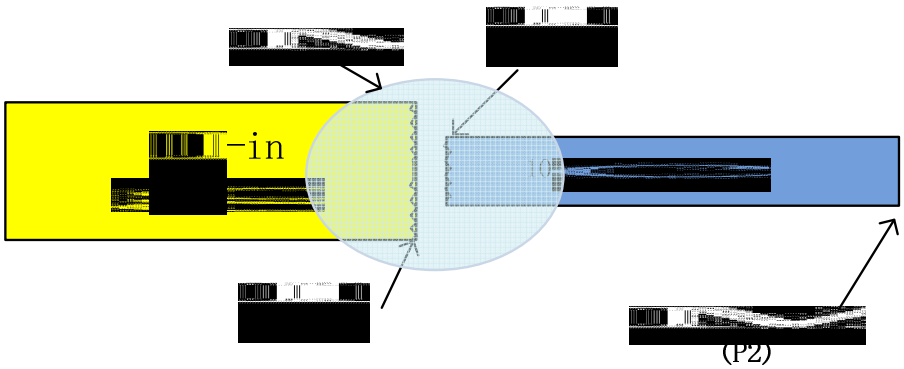

Figure 3.9. Machine polished SF endface with index matching oil

Table 3.3. The reflection power from laser-cut sapphire connection

Laser-cut sapphire end	GF/Air Air/C1 P2/Air	GF/Matching oil Matching oil/C1 P2/Air	GF/Air Air/C1 P2/ Acetone	GF/Matching oil Matching oil/C1 P2/Acetone
Reflection Power	-51.77dBm	-53.35 dBm	-53.306dBm	-59.42dBm

As the refractive index of air is 1 and acetone is 1.36, the theoretical reflectivity of P2/air and P2/acetone interface should be -11.28dB and -18.01dB respectively. Therefore, the reflection power should be reduced by 6.73 d B in theory after sapphire fiber immersed into the acetone. That is very close to the experimental value 6.11dB. Therefore, if the reflection power from connection point is denoted asP_c, the reflection power from sapphire fiber end in air (P2/air) is P_{sap}, the reflection power from P2/acetone is P_{sap_act} and the total reflection power collected in Port 3 is P_r, the following equations should be satisfied.

Sapphire end in air: $$P_r = P_{sap} + P_c = 10^{-\frac{53.30}{10}} \quad (3.4)$$

Sapphire end in acetone: $$P_{r1} = P_{sap\_act} + P_c = 10^{-\frac{59.42}{10}} \quad (3.5)$$

Therefore: $$P_{sap} - P_{sap\_act} = 10^{-\frac{53.30}{10}} - 10^{-\frac{59.42}{10}} = 3.5 \times 10^{-6} \quad (3.6)$$

The theory value : $$\frac{P_{sap}}{P_{sap\_act}} = 10^{\frac{6.73}{10}} = 4.71 \quad (3.7)$$

From (3.6)&(3.7):

We can get: $$P_{sap} = 4.48 \times 10^{-6} = -53.48dBm \quad (3.8)$$

$$P_{sap\_act} = 9.52 \times 10^{-7} = -60.2dBm \quad (3.9)$$

Therefore the reflection power from the connection point is:

$$P_c = 10^{-\frac{53.30}{10}} - P_{sap} = 1.91 \times 10^{-7} = -67.18dBm \qquad (3.10)$$

Based on the above calculation process, we can obtain the P_c with different connection conditions.

As Table 3.4 shows, the reflection power form connection point (P_c) was -43.36dBm for laser-cut sapphire fiber/laser-cut glass fiber connection. The reflection power from connection point was reduced to -53.31dBm by using laser-cut sapphire fiber. The power was further reduced to -67.18dBm when refractive index matching oil was applied. With laser-cut sapphire and matching oil, the connection reflection (P_c) has been reduced by at least 25dB compared with the polished sapphire fiber connection, and the reflection power from sapphire fiber end (P_{sap}) is about 14dB larger than the reflection power from connection point (P_c).

Table 3.4. Reflection power at different interfaces

	Polished Sapphire (P1) /Laser-cut glass fiber(GF)	Laser-cut sapphire (C1) / Laser-cut glass fiber(GF)	Laser-cut sapphire(C1)/ Laser-cut glass fiber (GF) immersed in RI oil
Reflection power from P2/air (P_{sap})	-53.92dBm	-57.03dBm	-53.48dBm
Reflection power from P2/acetone (P_{sap_act})	-60.07dBm	-63.76dBm	-60.20dBm
Totally measured reflection power when the sapphire end contacting with air(P_r)	-43.20dBm	-51.77dBm	-53.30dBm
Totally measured reflection power when the sapphire end contacting with acetone (P_{r1})	-43.50dBm	-52.93dBm	-59.42dBm
Reflection power from connection point P_c	-43.36dBm	-53.31dBm	-67.18dBm

It is concluded that the laser-cut sapphire fiber can help to reduce the DC power from connection point, and the matching oil can further weaken the undesirable reflection power.

3.3. DEVICE FABRICATION ON SINGLE CRYSTAL SAPPHIRE OPTICAL FIBER

The micro-square structure fabrication is carried out by a lab-made femtosecond laser micromachining system. The system consists of a femtosecond laser (Legend-F, Coherent, Inc.), optical parametric amplifier (OPA, Coherent Inc.), pulse shaper (Silhouette by Coherent, Inc.), beam delivery system, micro-vision system, and a five-axis high precision motion stage. The maximum output power, repetition rate, center wavelength and pulse width of the femtosecond laser are 1W, 1 kHz, 800 nm and 120 fs, respectively. The actual output power can be regulated accurately to a desired value through computer control. The femtosecond laser beam is directed into an objective lens and focused onto the subject mounted on a computer-controlled five-axis translation stage. The desired shape and dimensional parameters are input to the computer where the 3D solid model is generated.

The sapphire fiber is fixed on a precision translation stage, and laser beam is focused on the sapphire fiber surface to drill square hole layer by layer from one side to the other side. The average laser power is around 1.4mW. The size of the micro-structure is 40×40μm, precisely controlled by the computer controlled stage. In order to minimize blocking effect of the residue of sapphire fiber generated in fabrication process and get better square shape in every drilling layer, the laser fabrication process should be repeated several times. The image of HEIFPI structure fabricated by femtosecond laser, captured by scanning electron microscope (SEM), is displayed in Figure 3.10 (a) and (c).

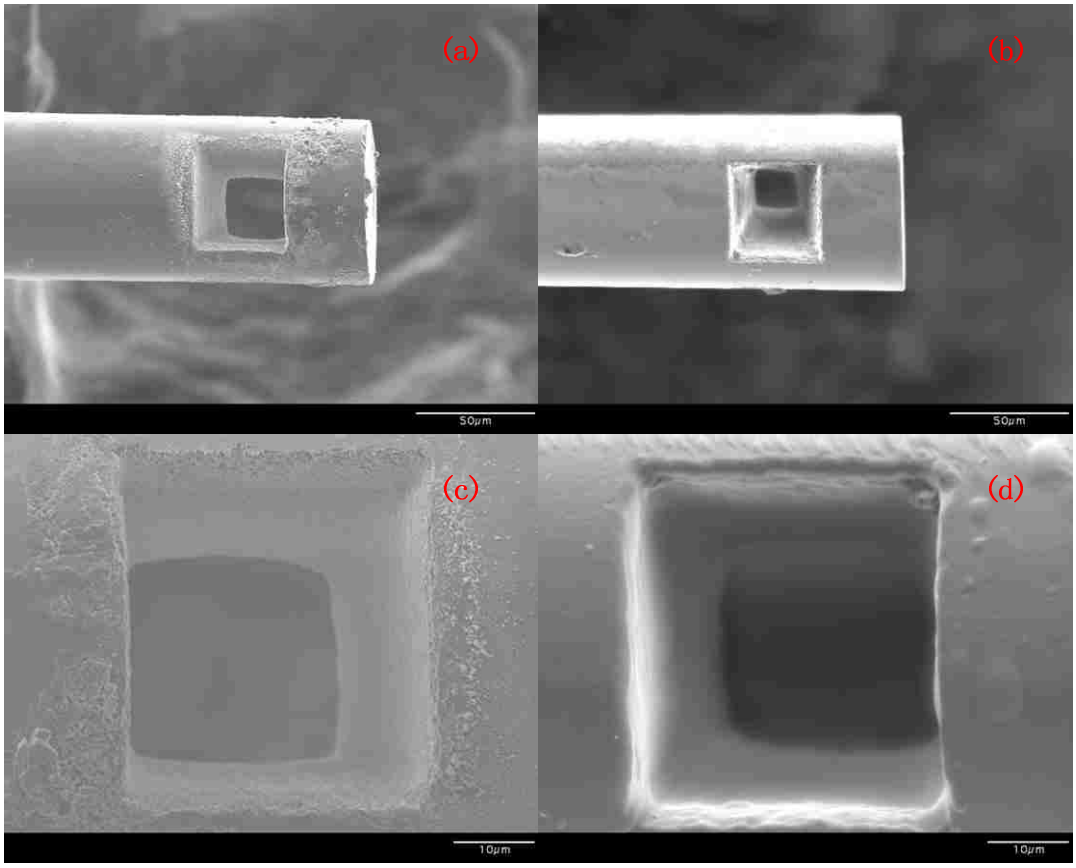

Figure 3.10. SEM image of HEIFPI. (a) (c)SEM images of HEIFPI before high temperature treatment (b) (d) SEM images of HEIFPI after high temperature treatment.

3.4. HIGH TEMPERATURE SURVIVABILITY TEST OF SAPPHIRE SENSOR

In order to test whether this micro-structured sapphire fiber-based sensor can survive in the extreme high temperature harsh environment, we put the sample into a bottom loading molydisilicide furnace (Deltech DT-31) which has a maximum temperature of 1650^{o}C. We then raise the temperature from room temperature (17^{o}C) to 1575 ^{o}C gradually, avoiding unexpected effects from sudden jump of temperature. The sample is supported by a 2.5mm×2.5mm sapphire plate and covered by a small crucible, which is used to prevent the sapphire fiber from blown away by accelerated air flow as temperature rises. After staying at 1575^{o}C for three days, the sample is taken out and coated with gold by sputtering machine (Desk V, Denton Vacuum) again for SEM. From

the SEM image of high temperature treated sample showed in Figure 3.10 (b) and (d), we can find that there is no visible change of HEIFPI structure. This result demonstrates that the HEIFPI fabricated on sapphire fiber can survive at temperature up to 1575^{o}C. The convex particles around the square hole fabricated on sapphire fiber have been significantly removed after high temperature treatment, and the HEIFPI structure seems much smoother than before high temperature treatment.

3.5. THE INTERFERENCE SIGNAL FROM HEIFPI

The ideal sapphire cavity is shown in Figure.3.11 (a). The walls of cavity are perfect parallel. The forward and backward rays propagate in counter-direction, and couple together to produce the interference spectrum. However, as shown in Figure 3.11 (b), the walls of femtosecond laser fabricated cavity are not parallel. The cavity has larger size on top and smaller size on bottom. That is because the focused laser beam has been partly blocked as the femtosecond laser go through the cavity during the fabrication. When using as a FP cavity, the propagating ray partially reflected back from the walls as Figure 3.11(b) shows. The light deviates from original ray path as the sapphire/air interfaces are not perpendicular to light propagating direction. It has severely decreased the visibility of interference spectrum of HEIFPI. And the highly multi-modes rays in sapphire fiber exacerbate this problem. The rays of different modes travel in sapphire fiber with different internal angle of reflection at sapphire/air interface, and feeds back different groups of interference signals. Based on the above reasons, the interference signals are very hard to be distinguished from the disordered reflection noise.

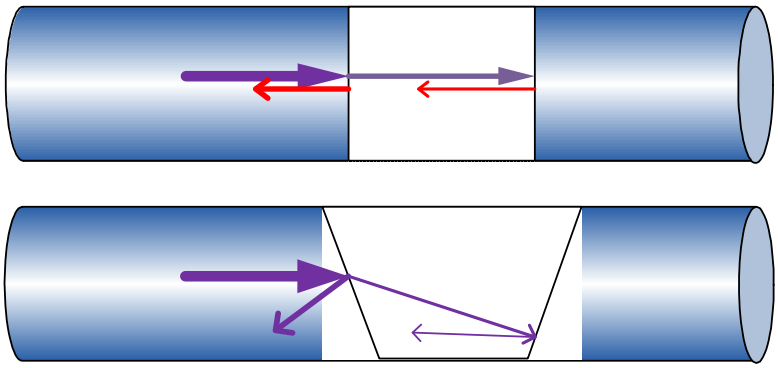

Figure 3.11. Ray propagation in EFPI. (a) The schematic of ray propagation in ideal EFPI (b) The schematic of ray propagation in lab-made EFPI

4. SUMMARY AND FUTURE WORK

4.1. BRIEF SUMMARY

In this thesis a double coating structure is proposed to improve the optical properties of sapphire fiber. The outer layer cladding material is chosen to be MgO because of its high melting temperature, high chemical and thermal stability, and low extinction coefficient. The high index material considered in this research is ceria (CeO_2) for its superior thermal durability. It also provides a chemical barrier/buffer layer to stabilize oxide interfaces at high temperatures. By far-field measurement technology, the MgO coating material has been proved to be able to reduce the NA Value of sapphire fiber. Under the same measurement condition, the NA values can be reduced by 25% at maximum. However, the MgO film coated directly on sapphire is not stable when the temperature exceeds 1000 ^{o}C. The MgO film reacts with sapphire during the one week heating process that caused the MgO/sapphire interface to disappear. Therefore, the inner coating layer, which stabilizes the chemical properties of coating material, is extremely important in high temperature application.

The femtosecond laser micro-fabrication technique was employed in HEIFPI sapphire sensor probe fabrication. The sapphire sensor cavity has a length of 40μm, and can survive in 1575 ^{o}C after three days high temperature treatment. As the reflection-type sensor sensitivity is limited by the DC reflection power induced from the sapphire/glass fibers interface, how to efficiently couple the light in the connection point becomes one of the most critical problems that need to investigate. The coupling issues have been divided into three parts: forward coupling efficiency, backward coupling efficiency, and interface DC limit. The forwards coupling efficiency is nearly 1, because the NA value and core diameter of lead-in glass fiber are much smaller compared with that of sapphire fiber. Backward coupling efficiency mainly depends on the core diameter and acceptance angle of lead-in fiber. Larger diameter lead-in fiber with higher NA value was found to capture more backward power. The DC limitation can be minimized by using polished sapphire and refractive index matching oil. With these methods, the reflection power has been reduced by 20dB according to our experimental results.

4.2. FUTURE WORK

As the MgO film directly coated on sapphire fiber is not stable when operating temperature exceeds 1000 OC, a barrier coating material must be investigated for higher temperature application. This part of work will be continued in the University of Cincinnati. Our group will continue help characterize the optical properties of the coating material.

Research is still on-going to improve the signal quality from a sapphire fiber sensor. Based on the work already done, the power from sensor needs to be increased and the reflection from the connection between the glass fiber and the sapphire fiber needs to be reduced. .

To increase the signal power from the sapphire EFPI, the walls need to be machined perpendicular to the fiber axis. This can be done with pre-adjust angles that match the numerical aperture of the focused femtosecond laser beam. In addition, curved wall shapes may help improve the optical power collections inside the cavity. It was found that the large number of supported modes in sapphire fiber is one of the major issues that caused the quality degradation of the interference spectrum. Therefore, in future, we will try to use collimator to reduce the excited modes during light coupling into the sapphire fiber. To reduce the reflection from the connection between the glass and sapphire fibers, it is suggested that an angle is engineered between the two fibers so that the endface reflections can be further reduced.

BIBLIOGRAPHY

[1] http://en.wikipedia.org/wiki/Optical_fiber Optical Fiber, August 2011.

[2] O. Schriever, "Electromagnetic waves in dielectric wires," *Annal.Physik*, 63(7), pp.645-673, 1920.

[3] K. C. Kao and G. A. Hockham, "Dielectric-fibre surface waveguides for optical frequencies," *Proc IEE*, 113, pp. 1151-1158, 1966.

[4] S.Takahashi and T. Kawashima, "Preparation of low loss multi-component glass fiber," *Tech. Dig. Int. Conf. Integr. Opt. and Opt. Fiber Commun.*, pp. 621, 1977.

[5] Rick k. Nubling and James A. Harrington H, "Optical properties of single crystal sapphire fibers," *Applied Optics*, Vol.36, No.23, 1997.

[6] Akio Makishima and John D.Mackenzie, "Calculation of bulk modulus, shear modulus and poisson's ratio of glass," *Journal of Non-crystalline solids*, Vol. 17, Issue.2, pp.147-157, 1974.

[7] "Considerations for improved bend performance optical fibers," *CORNING cable system LLC*, 2009.

[8] http://www.namiki.net/product/jewel/sapphire, single crystal sapphire, Namiki

[9] F. Benabid, M. Notcutt, L. Ju, and D.G.Blair , "Birefringence measurements of sapphire test masses for laser interferometer gravitational wave detector," Optics Communications, Vol.167, Iss1-6, pp. 7-13, 1999.

[10] S. C. Jones, B. A. M. Vaughan, and Y. M. Gupta, "Refractive indices of sapphire under elastic, uniaxial strain compression along the a axis," Journal of applied physics, Vol. 90, PP.4990.

[11] http://www.quartz-silica.net/sapphire.htm, Index of refraction for sapphire, Valley design corp.

[12] R.S. Feigelson, "Growth of fiber crystals," in: E. Kaldis (Ed.), "Crystal Growth of Electronic Materials," pp. 127, 1985.

[13] M.R.B. Andreeta, A.C. Hernandes, J., "Crystal Growth 200," pp621, 1999.

[14] V.V. Prokofiev, J.P. Andreeta, C.J. Lima, M.R.B. Andree-ta, A.C. Hernandes, J.F. Carvalho, A.A. Kamshilin, T.Jaaskelainen, J. "Crystal Growth," 137 (3–4) pp. 528–534. 1994

[15] Peter I. Antonov and Vladimir N. Kurlov, "A review of developments in shaped crystal growth of sapphire by the Stepanov and related techniques," Progress in Crystal Growth and Characterization of Materials, pp 63-122, 2002.

[16] D. H. Jundt, M. M. Fejer, and R. L. Byer, "Growth and optical properties of single-crystal sapphire fibers", SPIE,Vol.1048,Infrared of Fiber Optics,pp.39-43,1989

[17] L. M. Belyaev , "Ruby and Sapphire," Nauka Publishers, Moscow, Available From National Technical Info. Service, Springfield, VA 22161, (1974).

[18] Stephen C. Bates, "High Temperature Sapphire Fiber Cladding," Thoughtventions Unlimited, LLC.

[19] D. H. Jundt, M. M. Fejer, and R. L. Byer "Characterization of single-crystal sapphire fibers for optical power delivery systems" Appl. Phys. Lett. Vol.55, pp. 2170, 1989.

[20] Glenn N. Merberg and James A. Harrington , "Optical and mechanical properties of single-crystal sapphire optical fibers," Applied Optics, Vol.32, pp.3201, 1993.

[21] S..B. Desu, R.O. Claus, R. Raheem, and K.A. Murphy, "High Temperature Sapphire Optical Sensor Fiber Coatings," SPIE, Vol. 1307 ,Electro-Optical Materials for Switches, Coatings, Sensor Optics, and Detectors , 1990.

[22] M. Bass (Ed.), Handbook of Optics, Vol. 2: Devices, Measurements, and Properties, 2nd Ed., McGraw-Hill 1994.

[23] Desu, S. B. et al., " High temperature sapphire optical sensor fiber coatings," SPIE Int. Soc. Opt. Eng. Proc. SPIE Int. Soc. Opt. Eng. 1307: 2-9, 1990.

[24] J. Rennee Pedrazzani, Sapphire Optical Fibers Chaperter 21, pp.651-670

[25] C. A. Daniels, Ceramics structure and properties, pp. 156, 2002,

[26] M. Herzberger and C. D. Salzberg, J. Opr. SOC. Amer. 52,420 ,1962.

[27] R. E. Stephens and I. H. Malitson, 1. Research Nat. Bur. Siand. 49, no. 4, 249, 1952.

[28] M. J. Dodge, in "CRC Handbook of Laser Science and Technology," (M. J. Weber, Ed.), Vol. IV, CRC Press, Inc., Boca Raton, Florida, 31, 1986.

[29] David M. Roessler, Donald R. Huffman, Handbook of optical constants of solids II, pp. 919-955, 1998.

[30] Norton Company Refractories Division, Report #P-1.5-1, March 1, 1962.

[31] Francois Gervais, handbook of optical constants of solids II, 761-775, 1998.

[32] William J. Tropf, Michael E. Thomas, Handbook of optical constants of solids II, 883-897, 1998.

[33] NPL “Effective Area of Optical Fibers-Definition and Measurement Techniques”

[34] Ajoy Ghatak and K. Thyagarajan , “ Introduction in fiber optics ,” pp.416-422,1999.

[35] Corning Incorporated, “Numerical aperture measurement method”, pp.2, 2001.

[36] Ajoy Ghatak and K. Thyagarajan , “ Introduction in fiber optics ,” pp.422-432,1999.

[37] T. Giallorenzi, J. Bucaro, A. Dandridge, G. Sigel, J. Cole, S. Rashleigh, and R. Priest, "Optical fiber sensor technology," Quantum Electronics, IEEE Journal of **18**, pp.626-665 ,1982.

[38] B. Lee, "Review of the present status of optical fiber sensors," Optical Fiber Technology **9**, pp.57-79, 2003.

[39] T. Wei, Y. Han, Y. Li, H.-L. Tsai, and H. Xiao, "Temperature-insensitive miniaturized fiber inline Fabry-Perot interferometer for highly sensitive refractive index measurement," Opt. Express **16**, pp.5764-5769, 2008.

[40] Y. Li, C. R. Liao, D. N. Wang, T. Sun, and K. T. V. Grattan, "Study of spectral and annealing properties of fiber Bragg gratings written in H2-free and H2-loaded fibers by use of femtosecond laser pulses," Opt. Express **16**, pp.21239-21247 2008.

[41] R. R. Dils, "High-temperature optical fiber thermometer," Journal of Applied Physics **54**, 1198-1201,1983.

[42] H. Xiao, J. Deng, G. Pickrell, R. G. May, and A. Wang, "Single-Crystal Sapphire Fiber-Based Strain Sensor for High-Temperature Applications," J. Lightwave Technol. **21**, pp.2276 ,2003.

[43] J. Wang, B. Dong, E. Lally, J. Gong, M. Han, and A. Wang, "Multiplexed high temperature sensing with sapphire fiber air gap-based extrinsic Fabry?Perot interferometers," Opt. Lett. **35**, pp.619-621 ,2010.

VITA

Xia Fang was born in Hubei, China. In June 2006, she obtained a Bachelor's degree in Department of Physics from Huazhong University of Science and Technology, Hubei, China.

In December 2006, she enrolled in Hong Kong Polytechnic University, Hong Kong, China and start fiber research working there. She had published 4 Journal papers as first author during study in Hongkong. In January 2010, she joined the Phonic Technology Lab of Electrical and Computer Engineering Department, Missouri University of Science and Technology and began to purse her Master degree under the guidance of Dr. Xiao. She received her Master of Science Degree in Electrical Engineering in August 2012.